Precambrian Research 177 (2010) 308–322

Contents lists available at ScienceDirect

Precambrian Research

journal homepage: www.elsevier.com/locate/precamres

Peraluminous Grenvillian TTG in the Sierra de Pie de Palo, Western Sierras Pampeanas, Argentina: Petrology, geochronology, geochemistry and petrogenetic implications

Diego Morata[a,*], Brígida Castro de Machuca[b,c,1], Gloria Arancibia[d], Sandra Pontoriero[c], C. Mark Fanning[e]

[a] Departamento de Geología, Universidad de Chile, Plaza Ercilla 803, Santiago, Chile
[b] CONICET, Argentina
[c] Instituto de Geología (INGEO) y Departamento de Geofísica y Astronomía, FCEFN, Universidad Nacional de San Juan, Av. Ignacio de la Roza y Meglioli, C.P. 5407 Rivadavia, San Juan, Argentina
[d] Departamento de Ingeniería Estructural y Geotécnica, Pontificia Universidad Católica de Chile, Av. Vicuña Mackenna 4860, Santiago, Chile
[e] Research School of Earth Sciences, The Australian National University, Canberra, ACT 0200, Australia

ARTICLE INFO

Article history:
Received 23 January 2009
Received in revised form
12 November 2009
Accepted 4 January 2010

Keywords:
Granitoid
TTG
Isotopic geochemistry
Geochronology
Pie de Palo Complex
Western Sierras Pampeanas

ABSTRACT

Combined petrological, geochemical, isotopic and geochronological data shed light on the origin and evolution of a peraluminous garnet-bearing two-mica granitoid (El Tigre Granitoid: ETG) cropping out in southwestern Sierra de Pie de Palo (31°31′30″S–68°15′12″W), and to constrain the age and petrogenetic conditions of this intrusive event. ETG experienced amphibolite to greenschist facies metamorphism after igneous crystallization, followed by strong deformation restricted to narrow mylonite zones (ETG shear zone) and partial dynamic recrystallization under lower-T conditions. A dextral shear sense is compatible with kinematic observations registered along the NNE striking regional Las Pirquitas overthrust, active at 473 ± 10 Ma (K/Ar on <2 μm micaceous fraction for the ETG shear zone). The ETG crops out as small, tabular to lenticular vein-like bodies emplaced into metasedimentary rocks of the Pie de Palo Complex. The ETG ranges from granodiorite to tonalite, with a moderately peraluminous signature (ASI = 1.09–1.33; A/CNK >1.1; normative corundum; low CaO values between 1.72 and 2.41%), plotting mostly in the granite–trondhjemite fields of the Ab–An–Or diagram. The trace element contents show a relatively low abundance of Rb, HFS elements such as Y, Nb, Ta, Ga and Zr, and high concentrations of Ba, Sr, and $\sum$LREE. The chondrite-normalized REE pattern has a high slope with $[La/Yb]_N$ = 9.48–55.32 and a negative or absent europium anomaly. Relationships between trace elements suggest the classical setting of granitoids produced in a convergent plate setting.

A U–Pb SHRIMP crystallization age on zoned igneous zircon of 1105.5 ± 4.1 Ma suggests that the ETG could be part of the magmatic complex forming the Grenvillian basement of the Western Sierras Pampeanas. $(^{87}Sr/^{86}Sr)_{1105}$ values of 0.70543 and εNd of +4.2 indicate a rather immature source for its origin, with similar initial isotopic ratios to those found in orthogneisses from elsewhere in the Western Sierras Pampeanas. On the other hand, Sm–Nd model ages (T_{DM}) for the ETG range from 1.20 to 1.39 Ga. Geochemical and isotopic signatures of the ETG could be explained by low-pressure partial melting from a basaltic source under high geothermal gradient conditions. This thermal anomaly could be associated with the 1.1 Ga global period of enhanced mantle plume activity, developing widespread global magmatism.

1. Introduction

Arguments for a parautochthonous Gondwanan origin of the Cuyania terrane have been proposed by Finney (2007), who postulated that this terrane migrated during the Middle Ordovician along a transform fault at the southern margin of West Gondwana (present coordinates). Nevertheless, most studies carried out during the last two decades agree that the exotic Cuyania terrane was detached from Laurentia and coupled to Western Gondwana in the Early to Middle Ordovician (see Ramos, 2004 and references therein). The Cuyania terrane is well preserved in the basement rocks of the central Argentinean Andes as an elongated (≈1200 km long and up to 250 km wide) NNW-SSE area delimited by the Chilenia terrane to the west, the Pampia terrane to the east and

* Corresponding author. Tel.: +56 2 9784539; fax: +56 2 6963050.
E-mail addresses: dmorata@cec.uchile.cl (D. Morata), bcastro@unsj-cuim.edu.ar (B. Castro de Machuca), gloarancibia@gmail.com (G. Arancibia).
[1] Fax: +54 264 4265103.

0301-9268/$ – see front matter © 2010 Elsevier B.V. All rights reserved.
doi:10.1016/j.precamres.2010.01.001

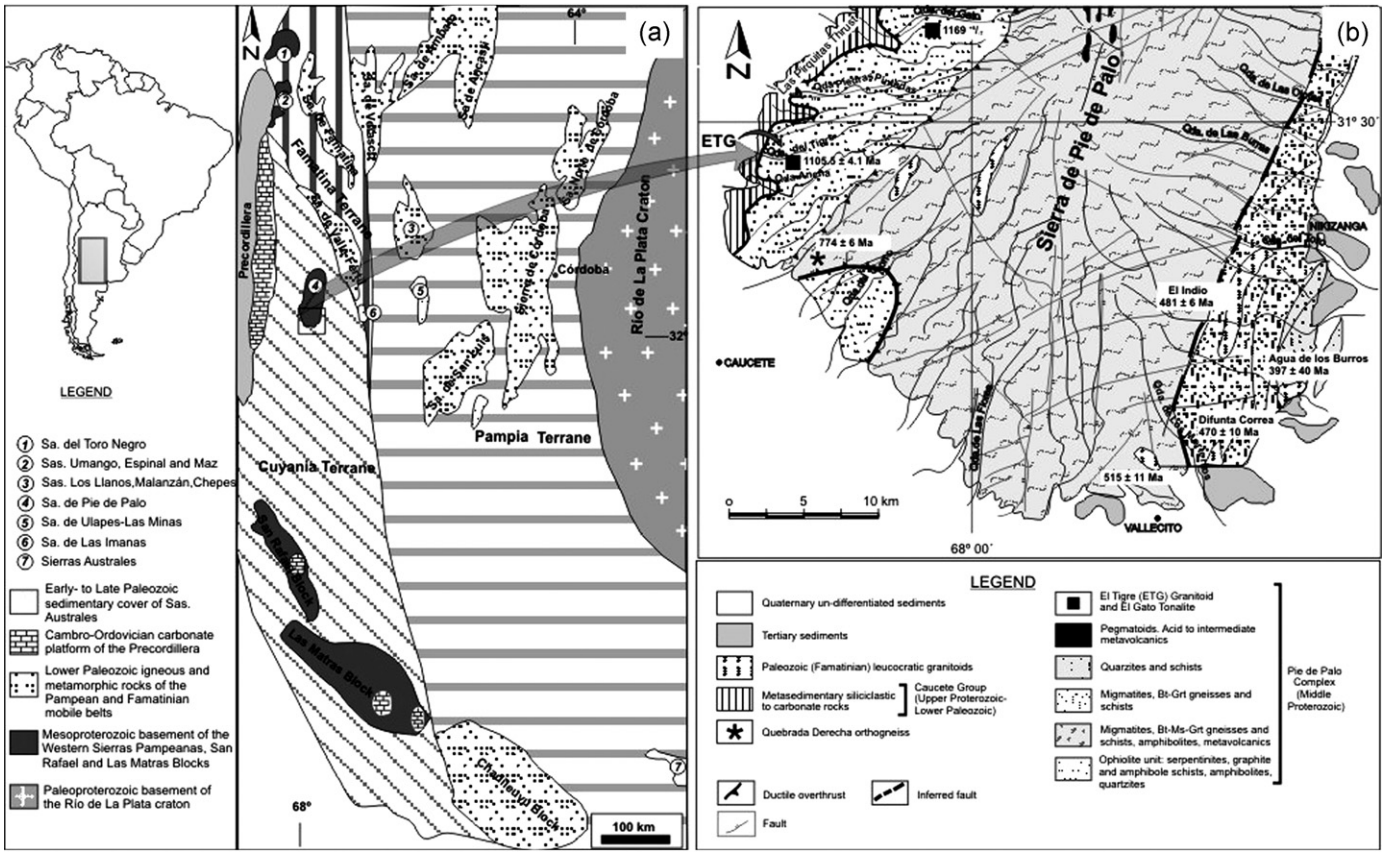

Fig. 1. (a) Sketch map of central Argentina showing the main tectonic domains, modified from Ramos (2004). Grenvillian ages were obtained from Sierra de Umango: 1108 ± 13 Ma and 1084–1189 Ma in orthogneiss, Varela et al. (2003, 2008); Sierra de Maz: 1070 ± 41 Ma in anorthosite, Casquet et al. (2004), Las Matras Block: ~1200 Ma in tonalite, Sato et al. (2000, 2004); Precordillera: xenoliths from Miocene lava domes, Kay et al. (1996); Sierra de Pie de Palo: carbonates, Galindo et al. (2004), 1021 ± 12 Ma in orthogneiss, Pankhurst and Rapela (1998); 1.4 Ga in detritic zircons, Casquet et al. (2001); Rapela et al. (2005); $1169^{+8/-7}$ Ma in tonalite, Vujovich et al. (2004). (b) Schematic geological map of southern Sierra de Pie de Palo (modified from Ramos and Vujovich, 2000 and Naipauer et al., 2005, 2009) showing the location of the El Tigre Granitoid (ETG), El Gato Tonalite ($1169^{+8/-7}$ Ma, Vujovich et al., 2004) and A-type granitoid (Quebrada Derecha orthogneiss, 774 ± 6 Ma, Baldo et al., 2006). El Indio and Difunta Correa plutons (481 ± 6 and 470 ± 10 Ma, Baldo et al., 2005) and other granitoid outcrops (Varela and Dalla Salda, 1993) are also indicated.

the Famatina terrane to the north (Ramos, 2004; Vaughan and Pankhurst, 2008). According to Ramos (2004), four sectors can be defined within the Cuyania terrane: the Precordillera Fold and Thrust Belt, the San Rafael Block, the Sierra de Pie de Palo area and the Las Matras Block (Fig. 1a).

Grenvillian ages have been obtained recently from U–Pb zircon dating both in plutonic rocks (e.g. Casquet et al., 2004; Sato et al., 2004; Vujovich et al., 2004) and metamorphic rocks (e.g. Pankhurst and Rapela, 1998; Casquet et al., 2001; Varela et al., 2003, 2008; Naipauer et al., 2005, 2009; Rapela et al., 2005) along the Western Sierras Pampeanas (Ramos, 1999) and even for xenoliths from Miocene lava domes (Kay et al., 1996) that crop out in the Argentinean Precordillera. Moreover, Sr and C isotopes obtained from some carbonate rocks in the Sierra de Pie de Palo (SPP) also indicate Grenvillian ages (Galindo et al., 2004). Recently Kumar et al. (2007) proposed a global thermal event at 1.1 Ga, probably driven by excess mantle heat, responsible for the development of widespread global magmatic activity. Consequently, this global thermal anomaly should be considered in the interpretation of the Grenvillian magmatic and metamorphic ages reported along the Western Sierras Pampeanas.

All these ages constitute direct or indirect evidence for the basement age of the terrane and, together with stratigraphic and sedimentological data (e.g. Astini et al., 1995; Keller, 1999), would support the hypothesis that this terrane could be derived from part of Laurentia. Consequently, the whole of the Western Sierras Pampeanas might represent basement remnants of an allochthonous Grenvillian terrane of which the Precordillera and the Sierra de Pie de Palo are only a part (see Pankhurst and Rapela, 1998, and references therein).

In this study we present radiometric ages (U/Pb SHRIMP ages on zircons, $^{40}Ar/^{39}Ar$ ages on biotite and muscovite and a K/Ar age on very fine-grained mica fraction) and the Rb/Sr and Sm/Nd signatures of a peraluminous garnet-bearing two-mica granitoid (El Tigre Granitoid: ETG) cropping out at the southwestern slope of the SPP (Fig. 1b). The aim of this study is to describe the mode of occurrence, petrography and chemistry of this granitoid and to correlate it with other granitoid rocks exposed in the area. Combined petrological, geochemical, isotopic and geochronological data presented here shed new light on its origin and evolution, and constrain the age of this intrusive phase emplacement. These data also help us to test whether the ETG could have formed part of a calc-alkaline arc that erupted during an inferred Grenvillian collision with the Mesoproterozoic basement of the Precordillera terrane (Vujovich and Kay, 1998), or whether it is related to the Early Ordovician peraluminous magmatism emplaced early during the Famatinian tectono-thermal event (Baldo et al., 2005).

2. Geologic setting

The SPP, one of the westernmost ranges in the west of the Sierras Pampeanas System, is considered by many authors (Astini et al., 1995; Casquet et al., 2001) as the main exposure of the Proterozoic basement of the Cuyania terrane, a supposed Laurentian

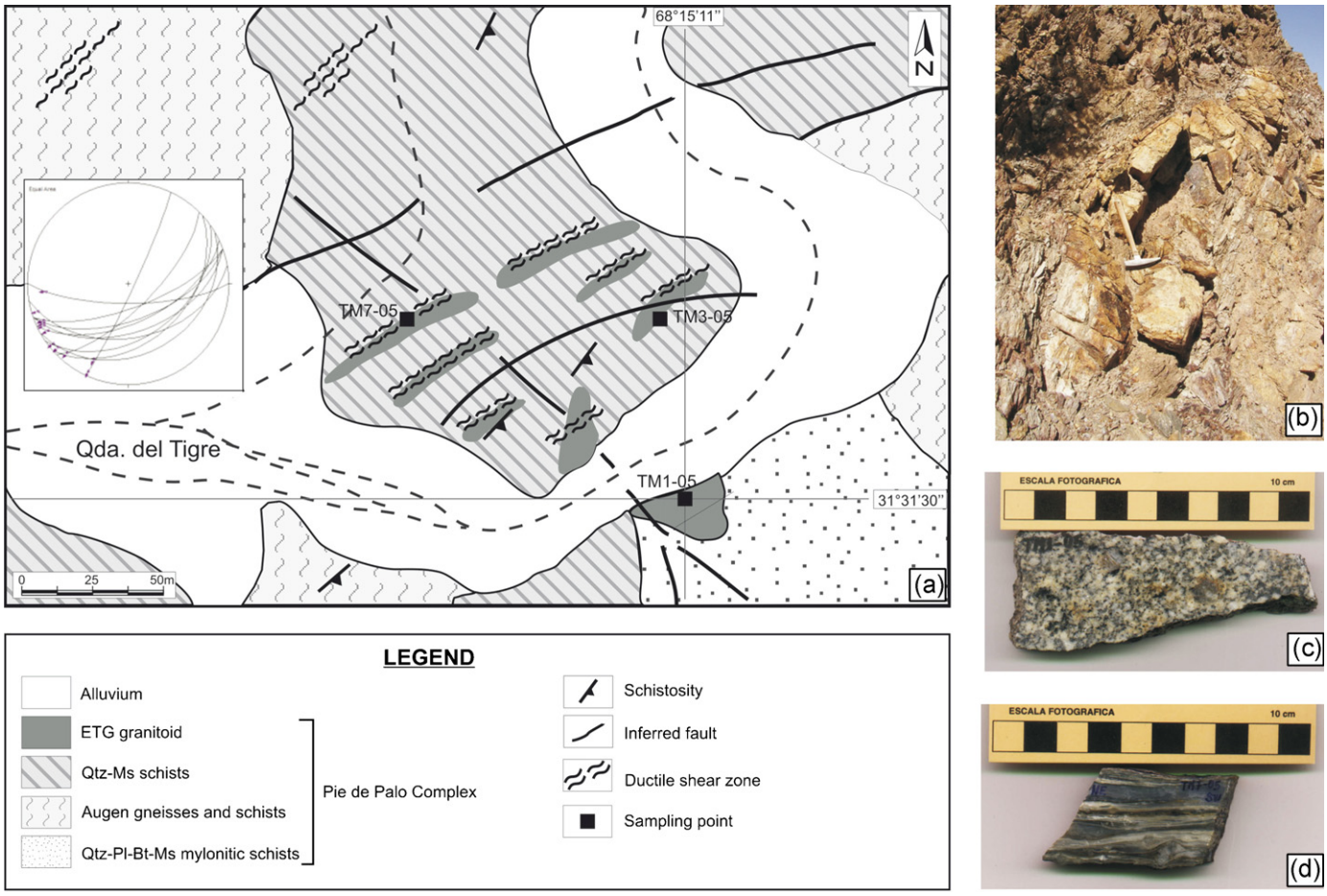

Fig. 2. (a) Detailed geological map and petrography of the ETG and its derived mylonites, with location of dated samples TM1-05 (undeformed ETG) and TM7-05 (ETG mylonite). Stereoplot (lower hemisphere) of the NE-E striking ETG shear zone with moderate southeasterly dip and subhorizontal stretching lineations. Arrows show the movement of the hanging wall (dextral shear). (b) Metric boudinage of El Tigre Granitoid inside metamorphic host rock. (c) Hand sample of undeformed/slightly deformed granitoid. (d) Hand sample of mylonitic/ultramylonitic rock.

exotic block accreted to the southwestern margin of Gondwana (its current location) in the Mid-Ordovician during the Famatinian orogeny (Thomas and Astini, 1996; Casquet et al., 2001; Ramos, 2004). The SPP comprises a tectonic collage of Mesoproterozoic mainly metasedimentary and igneous rocks and Neoproterozoic to Lower Paleozoic metasedimentary sequences (Vujovich et al., 2004 and references therein). It is composed of a metamorphic basement with two different sequences (Fig. 1b): the Pie de Palo Complex composed mainly of amphibolites and ultramafic rocks (mostly derived from island arc and oceanic environments) associated with biotite–muscovite–garnet gneisses and schists of Mid-Proterozoic age (Ramos and Vujovich, 2000), and the Caucete Group, in the western flank, characterized by platform siliciclastic to carbonate sequences possibly of late Proterozoic-Lower Cambrian age (Naipauer et al., 2009). Relationships between both complexes are always structural where exposed, represented by the first order Las Pirquitas Thrust along the western margin of the SPP (Fig. 1b). This thrust system, a NS-NNE trending low-angle and a top-to-the-west sense of relative movement, underwent protracted activity from 464 Ma until *ca.* 396 Ma, placing the Middle Proterozoic Pie de Palo Complex over the Upper Proterozoic–Lower Paleozoic Caucete Group (Ramos et al., 1998; Casquet et al., 2001). Nevertheless, recent $^{40}Ar/^{39}Ar$ ages in hornblende (Mulcahy et al., 2007) from a mylonite–ultramylonite of 515 ± 2 Ma and 510 ± 3 Ma have been interpreted as the earliest phase of deformation during thrusting (D_1, Van Staal et al., 2005). The *ca.* 464 Ma would then reflect the age of the penetrative deformation (D_2, Van Staal et al., 2005) related to the accretion of the Precordillera during the Middle Ordovician.

Granitic rocks of diverse nature and age that make up a small proportion of the crystalline basement of the SPP, have intruded the metamorphic basement (Fig. 1b). In the Pie de Palo Complex, a Mesoproterozoic (Grenvillian) age of 1.0–1.2 Ga was assigned based on Rb/Sr and U/Pb age determinations of some felsic meta-intrusive bodies present in the metasedimentary/metavolcanic middle to late Proterozoic sequences (McDonough et al., 1993; Varela and Dalla Salda, 1993; Pankhurst and Rapela, 1998). In the western SPP, close to the study area, a U–Pb SHRIMP age from zircon on a tabular, sill-like calc-alkaline tonalite/granodiorite ("El Gato tonalite") yielded an age of $1169^{+8/-7}$ Ma (Vujovich et al., 2004). Orthogneisses derived from metaluminous A-type monzogranites ("A-type granitoid") with a crystallization U–Pb SHRIMP zircon age of 774 ± 6 Ma were recognized by Baldo et al. (2006) in the southwestern SPP. Concerning Sr isotope compositions of the Difunta Correa Metasedimentary Sequence included in the Pie de Palo Complex (Baldo et al., 1998), the carbonates are coincident with those described for late Proterozoic carbonates and an age of middle to late Neoproterozoic (580–720 Ma) is inferred for them (Galindo et al., 2004; Rapela et al., 2005). Finally, two garnet-bearing two-mica granites, "El Indio" and the "Difunta Correa" plutons, with crystallization ages of 481 ± 6 Ma and 470 ± 10 Ma, respectively (U–Pb SHRIMP zircon ages), were also reported by Baldo et al. (2005) in the south-eastern part of the SPP (Fig. 1b).

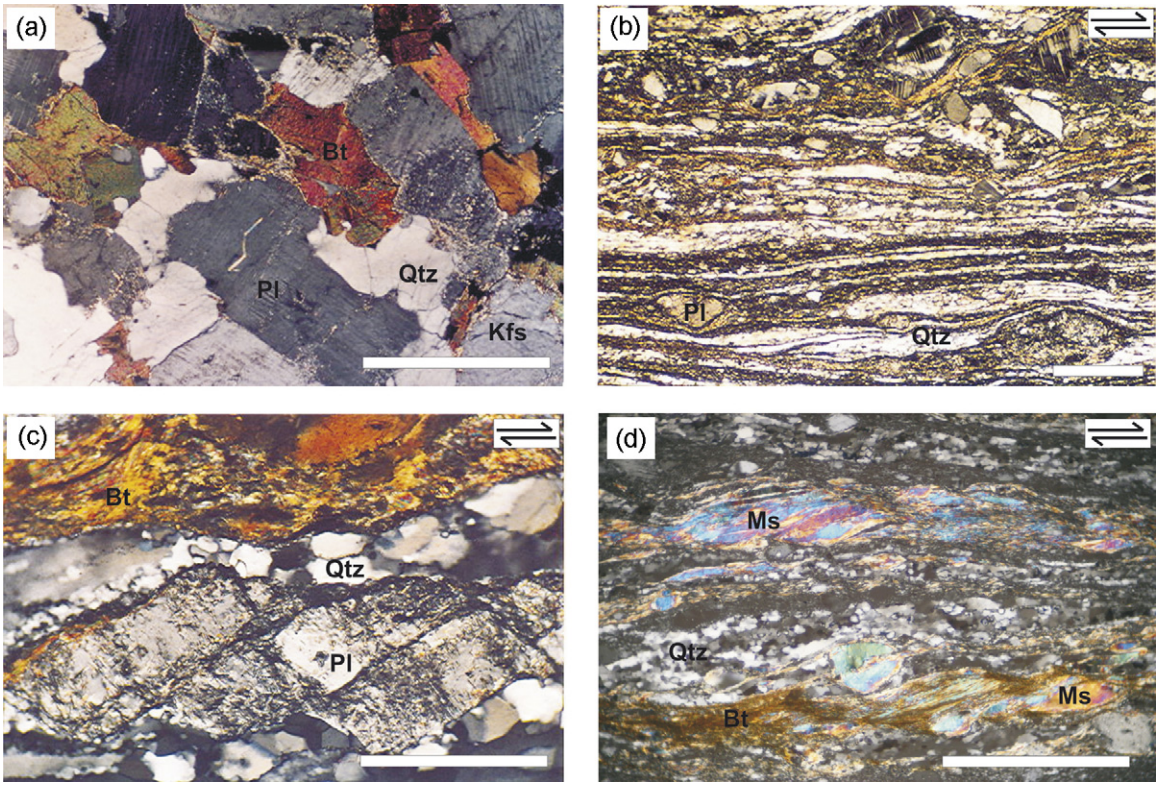

Fig. 3. Igneous and mylonitic microscopic textures of the ETG. (a) Allotriomorphic granular texture in undeformed tonalite (sample TM1-05) with plagioclase, quartz and biotite as main components (cross-polarized light). (b) Ultramylonitic texture in highly deformed granitoid sample TM7-05 (parallel-polarized light). (c) Plagioclase showing dextral brittle domino structure in a moderately deformed granitoid (cross-polarized light). (d) Dextral mica-fish structures developed in ultramylonitic rock (cross-polarized light). In all photographs, scale bar is 0.5 mm. Pl: plagioclase, Ms: muscovite, Bt: biotite; Qtz: quartz, Kfs: K-feldspar.

According to Casquet et al. (2001) the Pie de Palo Complex first underwent low-pressure/temperature (*P*/*T*) type metamorphism, reaching in some places migmatitic conditions (686 ± 40 MPa, 790 ± 17 °C), comparable to the Grenvillian M_2 metamorphism of the supposed Laurentian counterpart of the terrane. The second metamorphic event is of Famatinian age and took place under higher *P*/*T* conditions, following a clockwise *P*–*T* path (baric peak: 1300 ± 100 MPa, 600 ± 50 °C). Low-U zircon overgrew detrital Grenvillian cores as pressure fell from its peak, and yields U–Pb SHRIMP ages of *ca.* 460 Ma, which is interpreted as the age of ductile thrusting coincident with early uplift. The initial accretion to Gondwana must have occurred before this.

A tectonic model proposed by Vujovich and Kay (1998) for the SPP invokes a Mesoproterozoic oceanic suprasubduction zone setting for the Pie de Palo Complex that collided with a continental block during the Grenville orogeny. Collision was followed by formation of a Mesoproterozoic, dominantly felsic arc, whose magmas erupted through the thickened crust.

3. Petrology of the El Tigre Granitoid (ETG)

The ETG (31°31′30″S–68°15′12″W), is a homogeneous equigranular medium-grained (3–5 mm grain size) garnet-bearing two-mica granitoid occupying a restricted area at the downstream end of Quebrada del Tigre at the southwestern end of Sierra de Pie de Palo (Figs. 1 and 2). The ETG is contained in strongly folded and sheared rocks of the Pie de Palo Complex (Figs. 1b and 2a) and it is spatially closely associated with Las Pirquitas Thrust-related shear zones (Castro de Machuca et al., 2008).

Host rocks are low- to medium-grade metasedimentary rocks of the Mid-Proterozoic Pie de Palo Complex which locally consists of quartz–muscovite and quartz–plagioclase–biotite–muscovite ± garnet mylonite schists. Foliation of the host rocks varies greatly in orientation but has a NE average strike direction.

The granitoid crops out as small (10 cm to a few meters wide) tabular to lenticular light yellowish-gray felsic bodies emplaced concordantly with the schistosity of the metamorphic rocks. The ETG has been folded together with the country rock and as a result of rheology contrast, *boudinage* is frequently developed (Fig. 2b). The ETG is not foliated towards the outside of shear zones and contacts with the host rock are always sharp; both the ETG and the country rock are complexly folded at a regional scale. There is no evidence of contact metamorphism by the ETG and microgranular enclaves and xenoliths are absent.

Localized ductile shear zones, ranging in width from a few centimeters to a few meters, were observed in the ETG outcrops developed mainly at the boundaries of the granitoid *boudins*. Transition from undeformed/slightly deformed granitoid to mylonite–ultramylonite can be observed in the ETG ductile shear zones (Fig. 2c and d), allowing sample collection with relict textures related to an igneous and regional metamorphic event, and high-strained samples, related to the later shearing.

The ETG shear zone has a NE-E striking, moderately east-dipping mylonitic foliation, and subhorizontal stretching lineations (Fig. 2a). Mesoscopic and microscopic kinematic indicators suggest dextral shear sense compatible with NW-W shortening (Castro de Machuca et al., 2008). This is consistent with top-to-the-west N-S to NE striking ductile thrust along the western side of the SPP (Ramos et al., 1998; Vujovich et al., 2004; Mulcahy et al., 2007).

3.1. Igneous and metamorphic textures

The granoblastic texture of the ETG resembles the allotriomorphic granular texture of the original intrusive rock (Fig. 3a). Only

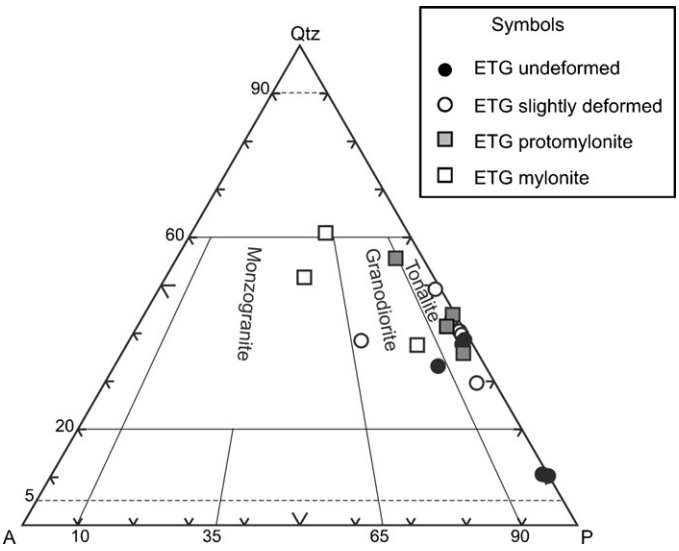

Fig. 4. Modal quartz (Qtz)-alkali feldspar (A)-plagioclase (P) ternary diagram (Streckeisen, 1976) of the ETG.

minor microscopic evidence of strain effects such as undulose extinction in quartz, some bending in micas and limited subgrain formation but no recrystallization is present.

Based on the modal classification (QAP diagram elaborated on a minimum of 1100 points per sample on thin sections, Fig. 4) the ETG composition varies from granodiorite to tonalite. Plagioclase (Ab_{87-73}, Michel-Levy method), quartz, biotite, subordinate (*ca.* 2.9% modal abundance increasing up to 15% modal abundance in quartz-rich lithologies) muscovite (Ms_1) and microperthitic K-feldspar in the granodioritic varieties, make up the bulk of the rock. Myrmekite patches sometimes replace the K-feldspar at the contact with plagioclase crystals. Polysynthetic twins in the myrmekite show that the quartz "worms" are in a plagioclase matrix. Rare muscovite–quartz symplectites are also found. Accessory minerals include abundant rutile, zircon, monazite and lesser allanite and ilmenite. Zircon crystals, some of them included in biotite, are mostly euhedral to subhedral (rounded); pleochroic radiation haloes can be visible around them. Rutile is present as deep golden-brown grains or as very fine needles within biotite. Rare apatite, titanite and tourmaline are also found.

Textural and mineralogical evidence suggest that after igneous crystallization the ETG underwent regional metamorphism that slightly obliterated primary igneous textures. Small subhedral to euhedral garnet crystals (0.06 mm average) with a pale green tint have been found in most of the samples. Relics of larger (up to 1.8 mm) anhedral garnets are partially replaced by chlorite, epidote and sometimes biotite along fractures and rimming garnet. Garnets up to 2.5 cm in diameter (in hand sample) surrounded by a leucocratic (Pl-Qtz) rim are also locally present. Its appearance suggests that they would have formed through metamorphic reactions under amphibolite facies conditions. Some samples contain no garnet but rounded clots of chlorite + epidote + opaques, allowing us to infer the former presence of garnet.

Abundant zoisite–clinozoisite + sericite derived from plagioclase and muscovite (Ms_2) from biotite, are assigned to retrogression events. Evidences for retrogression also include the partial replacement of garnet by biotite, biotite by secondary muscovite accompanied by iron–titanium oxide segregation, exsolution in feldspars, albitization of plagioclase and slight chloritization of biotite. In addition myrmekite formation generally records a partial adjustment to falling temperatures.

3.2. Mylonitic textures

Pronounced foliation and extensive grain-size reduction compared to the crystal size of the undeformed/slightly deformed ETG, characterize the more intense mylonitic deformation. A transition between protomylonite, mylonite and ultramylonite are observed in samples according to distance from shear zone centres. These rocks contain a variable proportion of plagioclase, K-feldspar and, more rarely, polycrystalline quartz porphyroclasts, in a fine-grained well-foliated, dynamically recrystallized quartz–phyllosilicate–epidote matrix (Fig. 3b).

Feldspar porphyroclasts tend to be elliptical or rounded in shape with strong evidence of fracturing and slipping along crystallographic cleavage planes, thus a bookshelf structure is common. Plagioclase porphyroclasts are usually fragmented, albitized and partially transformed to sericite and epidote. Secondary deformation twins are developed. Plagioclase shows evidence of brittle deformation by a "domino-type" (Passchier and Trouw, 2005) fragmented porphyroclast (Fig. 3c). Microcline porphyroclasts are relatively abundant; they are fractured in some cases and undulose extinction is common. Although cross-hatched twinning is also present, most microcline grains show deformation-enhanced twinning. A pressure-shadow texture composed of quartz, epidote and fine-grained white-mica is frequent around feldspar porphyroclasts.

When quartz porphyroclasts are present, they show strong undulose extinction, sutured boundaries, and become progressively flattened defining foliation and lineation. In mylonites and ultramylonites, quartz has developed as long and thin ribbons usually showing partial to full recovery.

Micas are severely bent and smeared out along foliation planes. Large mica flakes have developed characteristic "mica-fish" (Fig. 3d). Fractured garnet porphyroclasts are completely dismembered in fine-grained aggregates, and are not longer recognizable in the ultramylonites.

With increased strain, destruction of feldspar and micas is accompanied by a small but markedly greater abundance of fine-grained muscovite and epidote-group minerals, and hence probably indicates an increased water content of the total rock. Mica and epidote grains show preferred orientation and a relatively uniform grain size in the matrix. A lack of evidence for intracrystalline deformation in the smaller individual grains at the optical microscope scale, suggests that oriented new growth and/or dynamic recrystallization with recovering (e.g. Passchier and Trouw, 2005) could have occurred during shear deformation.

σ-Type feldspar porphyroclasts and mica-fish structures were used as kinematic indicators. Together with asymmetrical microfolds and microsheared porphyroclasts, a dextral (with minor normal component) shear movement can be inferred. These microtectonic data are consistent with meso-scale outcrop measurements (Fig. 2a). According to microstructure characterization, the metamorphic grade of the ETG shear zone reaches the greenschist facies.

4. U/Pb, Ar/Ar and K/Ar geochronology

4.1. U/Pb SHRIMP zircon ages

Zircons were separated from an undeformed granitoid (sample TM1-05) after crushing and standard heavy liquid and magnetic procedures at the Department of Geology (University of Chile). Twenty-two separated zircon grains were finally selected for determination of ion microprobe U–Th–Pb ratios, and the concentrations, analysed on SHRIMP II at the Australian National University, were determined relative to the Temora reference zir-

con. Decay constants employed are those recommended by Steiger and Jager (1977). Measured compositions were corrected for common Pb using the measured $^{204}Pb/^{206}Pb$ ratio.

The grains are in general small and were hand-picked with both elongate and more equant grain shapes selected for final analysis. Reflected and transmitted light photomicrographs and cathodo-luminescence (CL) images were captured with the aim of analysing the internal structure and possible zoning pattern of selected grains. Both elongate and more equant grain shapes show CL images with a mostly zoned igneous internal structure, although there are some small, more homogeneous areas that may indicate minor metamorphic overgrowths (Fig. 5a). Such areas were too small to be analysed in general by the 20 micron SHRIMP II spot. A summary of the analytical results is listed in Table 1.

Measured U contents range from 207 to 1024 ppm, with an average of 489 ppm, whereas Th ranges from 29 to 367 ppm, with a median of 158 ppm. Th/U ratios vary between 0.04 and 0.54, having an average value of 0.33. Common Pb ranges from 33 to 157 ppm, with an average value of 75 ppm and a proportion of ^{206}Pb in the total measured Pb (f_{204} in Table 1) less than 0.18%, the average of f_{204} being 0.06%. The data set uncorrected for common Pb plots close to concordia in a Tera–Wasserburg plot (Fig. 5b) in concordance with the low common Pb analysed. After correction for common Pb, the analyses are close to or within the analytical uncertainty of the Wetherill concordia diagram (Fig. 5c) giving a mean analytical age of $1103.0^{+10/-7.5}$ Ma (1σ, MSWD = 1.2), mostly forming a simple-bell shaped age distribution in $^{207}Pb/^{206}Pb$ ages (Fig. 5d). There is a slight skew to the younger side, and this may support a slightly younger overprint. The weighted mean for all $^{207}Pb/^{206}Pb$ ages has no excess scatter giving 1104.8 ± 4.8 Ma (1σ, MSWD = 1.2). If the youngest analysis is excluded then the weighted mean age is 1105.5 ± 4.1 Ma (1σ, MSWD = 1.02, probability = 0.44). Consequently, the dominant zoned igneous zircon in this rock crystallized at 1105 Ma.

4.2. $^{40}Ar/^{39}Ar$ biotite and muscovite ages

Single biotite and muscovite grains from the undeformed TM1-05 sample were selected for $^{40}Ar/^{39}Ar$ step heating dating. Micas were separated from this sample after crushing and final hand-picking selection under a binocular microscope from a 250–180 μm fraction. Sample preparation and $^{40}Ar/^{39}Ar$ mica analyses were carried out at the Laboratorio de Geocronología of the Servicio Nacional de Geología y Minería, Chile, following the analytical procedures detailed in Arancibia et al. (2006). After irradiation, samples were cooled for three months. Blanks obtained during the analysis were as follows: $^{40}Ar = 7.42 \times 10^{-17}$, $^{39}Ar = 4.51 \times 10^{-19}$, $^{38}Ar = 7.63 \times 10^{-20}$, $^{37}Ar = 8.13 \times 10^{-19}$, and $^{36}Ar = 2.44 \times 10^{-19}$ mol. $^{40}Ar/^{39}Ar$ analytical data of biotite (two runs) and muscovite from sample TM1-05 are listed in Table 2 and age spectra given in Fig. 6. Plateau, integrated and apparent ages in Table 2 are quoted at the 2σ level error. Plateau ages were calculated if more than 50% of the ^{39}Ar was released in at least three successive concordant (at the 2σ level) steps.

Two different runs on biotite separates were carried out, the first one giving a disturbed age spectrum pattern, without any plateau observed, progressively increasing apparent ages from step C to G from 946.9 ± 1.8 to 970.1 ± 15.1 Ma and a calculate integrated age of 938 ± 4 Ma (Table 2). An increase in the $^{37}Ar_{Ca}/^{39}Ar_K$ in the last steps (Table 2) probably corresponds to impurities in the biotite crystals.

For a second run on more carefully selected biotite crystals, without any optical evidence of microscopic impurities, the three first steps define a plateau age (50.2% ^{39}Ar released, MSWD 3.1, Table 2 and Fig. 6a) of 910 ± 20 Ma. The last three steps show a progressive increase in the apparent ages from 929.6 ± 2.8 to 950.3 ± 6.2 Ma, all eight steps forming an integrated age of 923 ± 4 Ma, which is consistent with the plateau age obtained for the same sample.

Muscovite grains present a highly disturbed pattern (Fig. 6b) and no plateaus were detected. In this disturbed apparent age pattern, two well defined sectors (step B *vs.* steps C–G) are observed with a progressive apparent age increasing from steps C (594.4 ± 1.3 Ma) to G (657.8 ± 3.0 Ma). It is worth noting that the apparent age obtained from step G is coincident (within the errors range) with the 653.9 ± 1.1 apparent age of step B (51.1% ^{39}Ar release on a single step). Steps C–F, characterized by lower apparent ages, could be interpreted as resulting from K-poor domains (higher Ca/K and Cl/K are detected on these three steps) or as consequence of a K-poor mixed phase in the muscovite grains. An integrated age of 641 ± 3 Ma is calculated.

4.3. K/Ar on fine-grained micaceous fraction

Two runs of the very fine-grained fraction (<2 μm) from the recrystallized micaceous mylonitic matrix were separated and analysed by the K/Ar method at the Laboratorio de Geocronología of the Servicio Nacional de Geología y Minería, Chile. X-ray diffraction on the separated fraction shows quartz–albite–muscovite and K-feldspar. Taking into account that mylonitic microstructures suggest shearing under greenschist facies conditions, the obtained age of 473 ± 10 Ma (Table 3) is interpreted as close in age to the mylonitic event (Castro de Machuca et al., 2008).

5. Geochemical characteristics

Thirteen fresh samples representative of textural and modal variations in the ETG were crushed, powdered and analysed at the ALS Chemex Laboratories in Vancouver, Canada (www.alschemex.com). Major elements were determined by standard X-ray fluorescence spectrometry after lithium borate fusion and trace elements, including rare earth elements (REE), by ICP-MS (Table 4). Instrumental uncertainties are as follows: all major elements ± 0.01%; Cs, Ho, Lu, Tb, Tm ± 0.01 ppm; Er, Eu, Sm, Yb ± 0.03 ppm; Dy, Gd, Th, U ± 0.05 ppm; Ga, Nd, Sr, Ta ± 0.1 ppm; Hf, Nb, Rb ± 0.2 ppm; Ba, Ce, Co, La, Y, Zr ± 0.5 ppm; Cu, Ni, Pb, V, Zn ± 5 ppm; Cr ± 10 ppm.

Most analyses form coherent arrays on major element Harker diagrams, with a decrease in TiO_2, FeOt, MgO, CaO and P_2O_5 with increasing SiO_2, while Na_2O increases slightly with silica. A more irregular pattern is observed for K_2O. The SiO_2 content of ETG samples ranges from 67.82 to 71.40% (average 70.4%), Al_2O_3 ranges from 14.70 to 16.07%, the Na_2O content varies between 3.55 and 4.79% and K_2O between 1.55 and 3.07%. The ETG plots in the subalkaline field on the total alkalis *vs.* silica diagram and clusters within the field of the calc-alkaline granites on the AFM diagram. According to the normative composition, the ETG mostly plots in the granite–trondhjemite fields on the Ab–An–Or diagram (Fig. 7a), independent of the deformational stage.

In terms of alumina saturation, the ETG classified as slightly to moderately peraluminous (Fig. 7b), with alumina saturation index (ASI) values ranging from 1.09 to 1.34 (average of 1.22). The peraluminous character is also indicated by the presence of normative corundum content (average of 2.89%) and low CaO values between 1.72 and 2.41%. The occurrence of subordinate primary muscovite and the presence of metamorphic garnet could also be evidence of its peraluminous nature, but its significance will be discussed later.

The relationship between Ga/Al and (Ce + Zr + Nb + Y) indicates that the ETG belongs to the S- or I-type, contrasting with an A-type granitoid (Quebrada Derecha orthogneiss) found by Baldo et al. (2006) few kilometers south of the ETG (Figs. 1b and 8a).

Table 1
Summary of SHRIMP U–Pb zircon results for sample TM1-05, ETG, Sierra de Pie de Palo, Western Sierras Pampeanas, Argentina.

Grain spot	U (ppm)	Th (ppm)	Th/U	$^{206}Pb^*$ (ppm)	$^{204}Pb/^{206}Pb$	f_{206} (%)	Total ratios				Radiogenic ratios						ρ	Age (Ma)				% Disc
							$^{238}U/^{206}Pb$	±	$^{207}Pb/^{206}Pb$	±	$^{206}Pb/^{238}U$	±	$^{207}Pb/^{235}U$	±	$^{207}Pb/^{206}Pb$	±		$^{206}Pb/^{238}U$	±	$^{207}Pb/^{206}Pb$	±	
1.1	249	104	0.42	40	0.000004	0.01	5.332	0.060	0.0770	0.0005	0.1875	0.0021	1.990	0.026	0.0770	0.0005	0.869	1108	11	1120	13	1
2.1	409	147	0.36	63	0.000028	0.05	5.609	0.060	0.0766	0.0004	0.1782	0.0019	1.872	0.022	0.0762	0.0004	0.895	1057	10	1101	11	4
3.1	328	105	0.32	48	0.000099	0.17	5.837	0.063	0.0778	0.0004	0.1710	0.0018	1.801	0.024	0.0764	0.0006	0.821	1018	10	1105	15	8
4.1	282	91	0.32	44	0.000017	0.03	5.508	0.077	0.0767	0.0005	0.1815	0.0025	1.915	0.030	0.0765	0.0005	0.905	1075	14	1109	13	3
5.1	634	232	0.37	98	0.000007	0.01	5.575	0.058	0.0762	0.0003	0.1793	0.0019	1.881	0.021	0.0761	0.0003	0.929	1063	10	1097	8	3
6.1	680	367	0.54	104	0.000013	0.02	5.595	0.059	0.0764	0.0003	0.1787	0.0019	1.877	0.021	0.0762	0.0003	0.934	1060	10	1100	8	4
7.1	254	105	0.41	40	–	<0.01	5.474	0.060	0.0769	0.0005	0.1827	0.0020	1.938	0.025	0.0769	0.0005	0.867	1082	11	1119	13	3
8.1	746	29	0.04	113	0.000032	0.05	5.661	0.059	0.0771	0.0003	0.1765	0.0018	1.865	0.021	0.0766	0.0003	0.928	1048	10	1111	8	6
9.1	320	45	0.14	49	0.000080	0.13	5.568	0.060	0.0763	0.0004	0.1794	0.0019	1.858	0.024	0.0751	0.0006	0.824	1063	11	1072	15	1
10.1	354	160	0.45	57	0.000011	0.02	5.334	0.059	0.0758	0.0005	0.1874	0.0021	1.954	0.026	0.0756	0.0006	0.835	1107	11	1084	15	−2
11.1	415	118	0.28	65	0.000028	0.05	5.501	0.058	0.0763	0.0004	0.1817	0.0019	1.903	0.023	0.0760	0.0004	0.891	1076	11	1094	11	2
12.1	207	82	0.40	33	0.000030	0.05	5.388	0.060	0.0762	0.0005	0.1855	0.0021	1.938	0.027	0.0758	0.0007	0.790	1097	11	1089	17	−1
13.1	339	123	0.36	53	0.000007	0.01	5.497	0.059	0.0766	0.0004	0.1819	0.0020	1.919	0.023	0.0765	0.0004	0.885	1077	11	1109	11	3
14.1	566	255	0.45	87	–	<0.01	5.556	0.058	0.0768	0.0003	0.1800	0.0019	1.907	0.022	0.0768	0.0003	0.924	1067	10	1117	9	5
15.1	504	191	0.38	78	0.000073	0.12	5.581	0.059	0.0771	0.0003	0.1790	0.0019	1.877	0.022	0.0761	0.0004	0.898	1061	10	1097	10	3
16.1	673	335	0.50	112	0.000028	0.05	5.172	0.054	0.0767	0.0003	0.1933	0.0020	2.034	0.023	0.0763	0.0003	0.931	1139	11	1104	8	−3
17.1	1024	259	0.25	157	0.000010	0.02	5.622	0.058	0.0762	0.0002	0.1778	0.0018	1.864	0.020	0.0760	0.0002	0.962	1055	10	1095	6	4
18.1	465	171	0.37	70	0.000105	0.18	5.692	0.060	0.0785	0.0003	0.1754	0.0018	1.862	0.022	0.0770	0.0004	0.877	1042	10	1121	12	7
19.1	482	150	0.31	74	0.000007	0.01	5.582	0.060	0.0772	0.0004	0.1791	0.0019	1.904	0.022	0.0771	0.0004	0.903	1062	10	1124	10	5
20.1	707	117	0.16	110	0.000005	0.01	5.501	0.060	0.0765	0.0003	0.1818	0.0020	1.917	0.022	0.0765	0.0003	0.954	1077	11	1108	7	3
21.1	902	231	0.26	131	0.000100	0.17	5.910	0.061	0.0780	0.0002	0.1689	0.0017	1.785	0.020	0.0766	0.0003	0.924	1006	10	1111	9	9
22.1	220	59	0.27	34	0.000026	0.04	5.610	0.064	0.0769	0.0005	0.1782	0.0020	1.879	0.025	0.0765	0.0005	0.851	1057	11	1108	14	5

Notes: (1) Uncertainties given at the 1σ level.
(2) Error in Temora reference zircon calibration was 0.45% for the analytical session (not included in above errors but required when comparing $^{206}Pb/^{238}U$ data from different mounts).
(3) Pb^* is the radiogenic Pb.
(4) f_{206}% denotes the percentage of ^{206}Pb that is common Pb.
(5) Correction for common Pb made using the measured $^{204}Pb/^{206}Pb$ ratio.
(6) For % Disc, 0% denotes a concordant analysis.

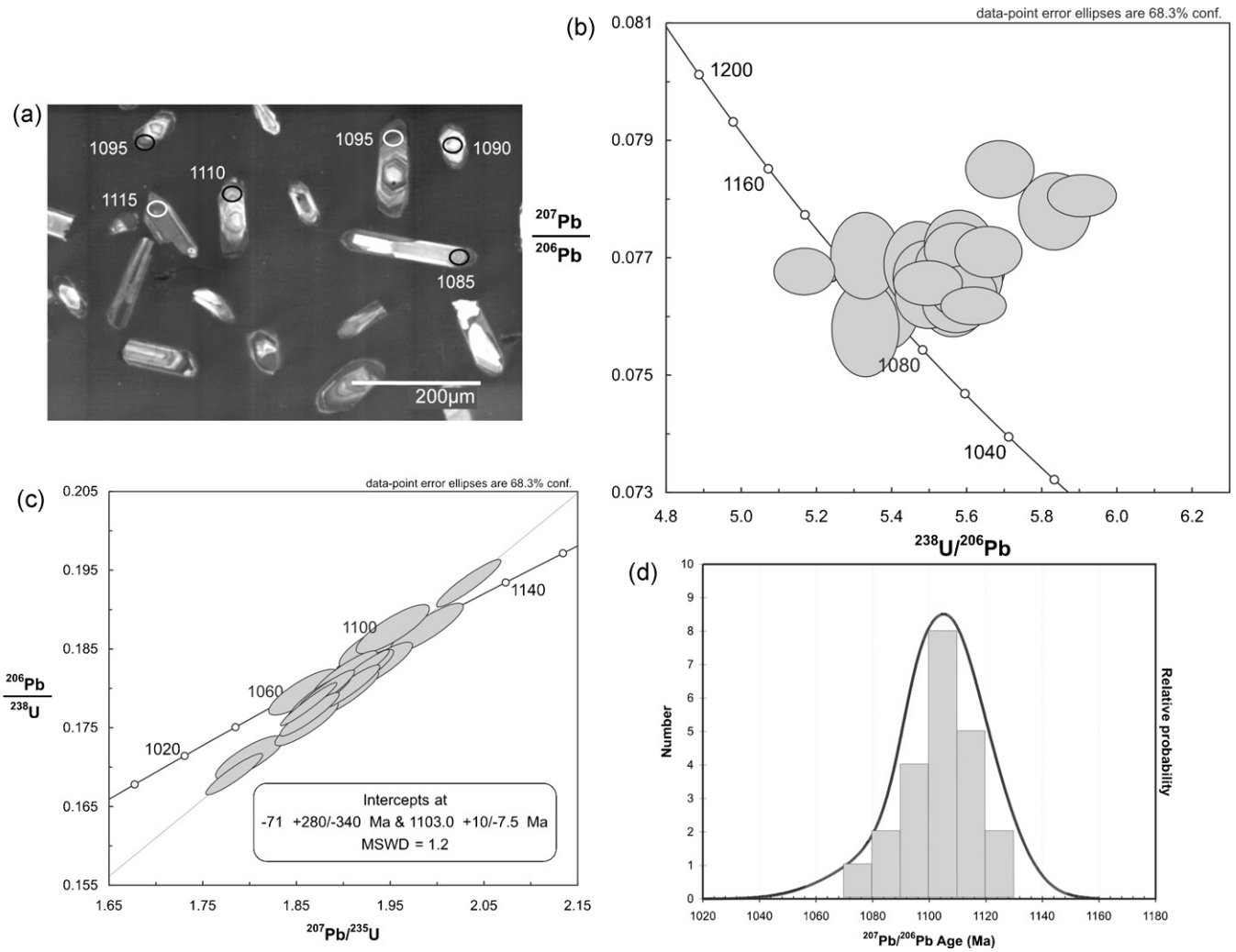

Fig. 5. (a) Zircon cathodo-luminescence (CL) image and U–Pb radiometric ages for sample TM1-05 (ETG, Sierra de Pie de Palo, Western Sierras Pampeanas, Argentina). (b) Tera–Wasserburg diagram and (c) Wetherill plot of the full dataset showing error ellipses at 68.3% confidence limits for igneous cores. (d) Relative probability plot of full data showing the homogeneous age of analysed zircons.

The trace element contents show a relatively low abundance of Rb (56.2–83.0 ppm), HFS elements such as Y (6.1–31.5 ppm), Nb (4.3–6.4 ppm), Ta (0.3–0.5 ppm), Ga (17.7–21.2 ppm) and Zr (205–491 ppm), and high concentrations of Ba (354–1770 ppm), Sr (264–568 ppm), and ΣLREE (136–211 ppm). The ETG contents of high-field strength elements (HFSE) are relatively low, which is typical of orogenic granites, with very low Rb/Sr and Sr/Ba ratios (0.13–0.28 and 0.17–0.89, respectively). The low Y and Zr values are probably controlled by the accessory zircon, rutile, allanite, monazite and apatite which commonly retain these elements and affect thus their concentrations. The relationships between trace elements suggest that the ETG has the classical setting of granitoids produced in a convergent plate environment (e.g. Pearce et al., 1984). In fact, the ETG plots in the volcanic arc granite field on the Y + Nb *vs.* Rb diagram (Fig. 8b). This tectonic environment is also confirmed by the Ta + Yb *vs.* Rb, Yb *vs.* Ta and Hf–Rb/10 − Ta × 3 discrimination diagrams for granites. According to the relationships between trace elements, the ETG could be considered as a volcanic arc granitoid emplaced in a convergent plate setting under a compressive tectonic regime.

A chondrite-normalized REE pattern (Fig. 9) shows a high slope with $[La/Yb]_N$ = 9.48–55.32 and a negative to slightly positive europium anomaly (Eu/Eu^* = 0.62–1.10). A slight decrease in the total REE amounts, but preserving a parallel pattern, is observed when comparing the normalized pattern of undeformed or slightly deformed granitoids with highly deformed mylonites (Fig. 9a). This REE mobilization during mylonitization could be related to a decrease of the modal garnet and accessory mineral amounts in mylonites compared with undeformed rocks. The strong difference in the REE pattern of the ETG with respect to the El Gato tonalite (Fig. 9b) is also remarkable; this is characterized by a very low HFSE ratio and low HREE, and was interpreted by Vujovich et al. (2004) to be a consequence of the derivation of this rock from an oceanic rather than a continental setting. Nevertheless, a similitude in the REE normalized pattern as well as with the Yb_N values are observed between the ETG and tonalites from the Mesoproterozoic basement of the Las Matras Block (Fig. 9b), suggesting similar petrogenetic processes as discussed latter below.

6. Sr- and Nd-isotopes

Rb/Sr and Sm/Nd isotopic analyses were carried out on whole rock samples at the Geochronological Research Center, University of São Paulo, Brazil. The Rb–Sr and Sm–Nd analyses were prepared using the procedures of Tassinari et al. (1996) and Sato et al. (1995), which involve HF-HNO_3 dissolution plus HCl cation exchange separation. No visible solid residues were observed after dissolution.

Table 2
$^{40}Ar/^{39}Ar$ step heating analytical data of biotite (two runs) and muscovite from sample TM1-05, ETG, Sierra de Pie de Palo, Western Sierras Pampeanas, Argentina.

Step	Laser power	Ca/K	Cl/K	$^{36}Ar/^{39}Ar$	$^{40}Ar^*/^{39}Ar$	Mol ^{39}Ar	Cum. %	$\%^{40}Ar^*$	Age (Ma)	($\pm 2\sigma$)
Run 11436-01, biotite, sample TM1-05 ($J = 0.0013212 \pm 0.0000027, 2\sigma$)										
A	3	0.028	0.006	0.022	492.334	0.797	10.0	98.7	903.9	2.5
B	6	0.009	0.009	0.008	522.403	2.764	44.8	99.6	946.9	1.8
C	9	0.015	0.013	0.008	511.804	1.663	65.7	99.5	931.8	2.8
D	12	0.009	0.008	0.007	516.340	1.546	85.2	99.6	938.3	1.8
E	15	0.016	0.006	0.006	521.030	0.656	93.5	99.7	944.9	3.3
F	20	0.034	0.007	0.006	529.269	0.402	98.5	99.7	956.5	3.4
G	25	0.031	0.015	0.007	538.968	0.082	99.5	99.6	970.1	15.1
H	30	−0.077	0.025	0.004	531.476	0.036	100.0	99.8	959.6	23.7
Integrate age = No plateaus detected									938	4
Run 11436-02, biotite, sample TM1-05 ($J = 0.0013212 \pm 0.0000027, 2\sigma$)										
A*	3	0.075	0.016	0.024	496.701	0.687	11.2	98.6	910.2	2.8
B*	6	0.013	0.006	0.007	502.689	1.596	37.3	99.6	918.8	2.4
C*	9	0.037	0.014	0.009	498.151	0.788	50.2	99.5	912.3	2.7
D	12	0.035	0.011	0.006	508.936	1.009	66.7	99.6	927.8	2.4
E	15	0.017	0.006	0.006	509.075	0.844	80.5	99.6	928.0	2.6
F	20	0.018	0.002	0.003	510.258	0.573	89.9	99.8	929.6	2.8
G	25	0.062	0.005	0.006	518.160	0.362	95.8	99.7	940.9	3.9
H	30	−0.033	0.016	0.007	524.857	0.258	100.0	99.6	950.3	6.2
Integrate age =									923	4
(*) Plateau Age =									910	20
Run 11437-01, muscovite sample TM1-05 ($J = 0.0013224 \pm 0.0000027, 2\sigma$)										
A	3	1.422	−0.018	0.098	479.717	0.062	0.9	94.3	886.3	9.9
B	6	0.019	0.006	0.008	330.339	3.441	52.0	99.3	653.9	1.1
C	9	0.056	0.012	0.006	295.110	1.338	71.8	99.4	594.4	1.3
D	12	0.057	0.007	0.005	313.827	0.421	78.1	99.5	626.3	2.6
E	15	0.047	0.006	0.002	319.172	0.488	85.3	99.8	635.3	2.3
F	20	0.034	0.010	0.001	327.829	0.596	94.2	99.9	649.7	2 2
G	25	0.069	0.001	0.004	332.696	0.369	99.6	99.6	657.8	3.0
H	30	0.471	0.062	0.018	295.576	0.024	100.0	98.3	595.2	20.3
Integrate age = No plateaus detected									641	3

Step: laser output power (in watt) for analysed micas. $^{40}Ar^*$ is the radiogenic argon from natural K-decay.

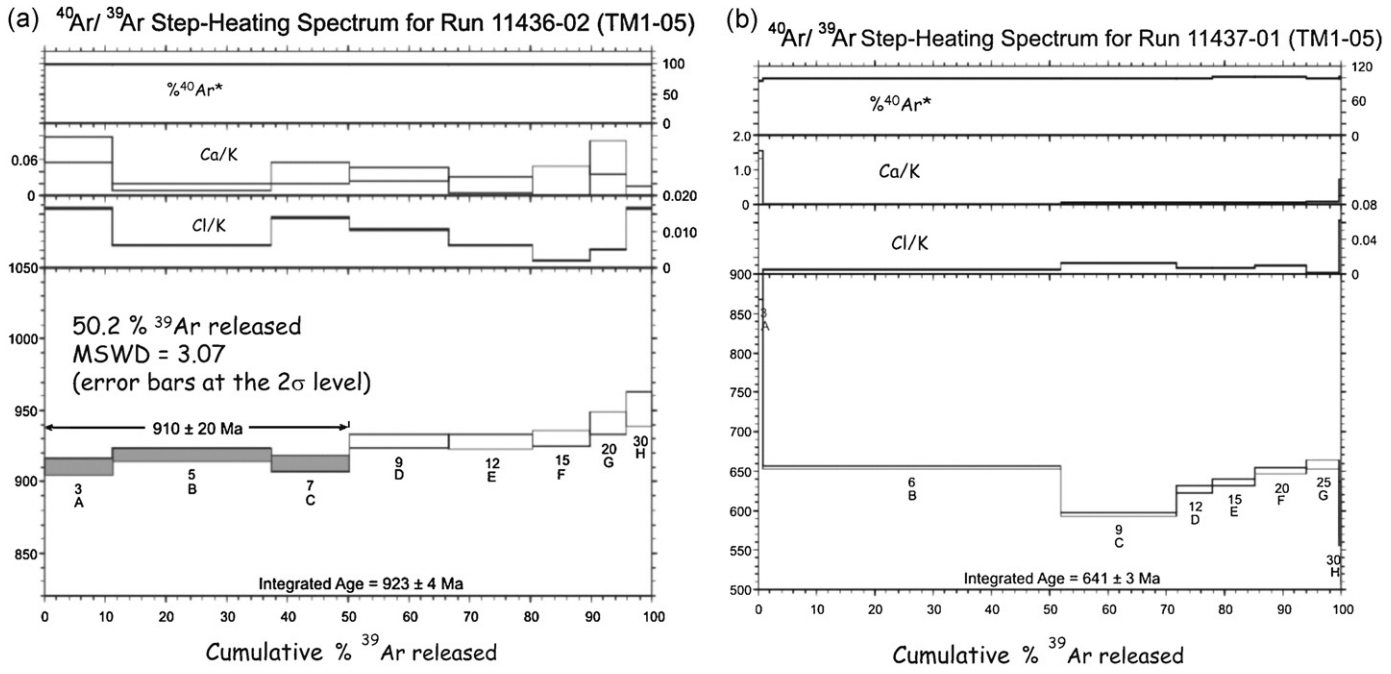

Fig. 6. $^{40}Ar/^{39}Ar$ step heating apparent age spectra and $\%^{40}Ar^*$, $^{37}Ar_{Ca}/^{39}Ar_K$ and $^{36}Ar_{Cl}/^{39}Ar_K$ spectrum of selected biotite (a) and muscovite (b) grains from sample TM1-05 (ETG, Sierra de Pie de Palo, Western Sierras Pampeanas, Argentina).

Table 3
Analytical results of K/Ar dating (sample TM7-05 ETG mylonite), Sierra de Pie de Palo, Western Sierras Pampeanas, Argentina.

Sample	Lab. number	Dated material	%K	Rad. Ar (nl/g)	Atmosph.	Age (Ma)	Error (2σ)
TM7-05	P900-TM7	<2 μm micaceous fraction	3.130	65.755	6	473	±14
TM7-05	P894-TM7	<2 μm micaceous fraction	3.130	65.877	9	473	±14
Weighted average						473	±10

Table 4
Major and trace elements analyses of the El Tigre Granitoid (ETG), Sierra de Pie de Palo, Western Sierras Pampeanas, Argentina. Major oxides in wt%, trace elements in ppm. Fe_2O_3 represents total Fe.

Sample	S15	S27	TM1-05	S4S	S15S	TM3-05	TM6-05	S21	TM4-05	TM2-05	SIS	T39	TM7-05
Rock type	Prl	Prl	Prl	Prl	Prl	Sd	Sd	Sd	Prm	Myl	Myl	Myl	Myl
SiO_2	67.82	68.78	68.95	71.40	69.10	68.49	69.78	70.50	70.03	74.47	71.20	70.66	73.49
TiO_2	0.53	0.35	0.51	0.47	0.46	0.56	0.42	0.40	0.39	0.11	0.48	0.25	0.11
$A1_2O_3$	15.72	15.68	16.03	15.60	15.80	16.07	15.70	14.70	15.08	14.40	15.90	15.38	14.94
Fe_2O_3	3.46	2.70	3.42	2.58	2.61	3.84	2.90	2.98	2.89	1.05	2.42	2.03	1.44
MnO	0.03	0.02	0.06	0.05	0.04	0.04	0.02	0.03	0.02	0.02	0.04	0.02	0.02
MgO	0.91	0.71	0.92	0.81	0.89	0.89	0.71	0.77	0.76	0.16	0.80	0.48	0.22
CaO	2.28	1.98	2.19	2.39	2.39	2.17	2.41	1.72	2.08	1.10	1.76	1.43	1.50
Na_2O	3.64	3.82	4.30	4.79	4.25	3.73	3.55	3.61	3.83	4.19	4.48	3.74	4.03
K_2O	2.79	2.96	1.76	1.55	2.97	1.86	2.34	3.07	1.76	1.74	1.81	3.69	3.17
P_2O_5	0.11	0.10	0.07	0.10	0.12	0.07	0.09	0.07	0.10	0.08	0.08	0.07	0.07
LOI	0.91	0.89	0.65	0.40	1.25	1.10	1.01	1.01	1.20	0.86	1.40	0.81	0.69
Total	98.41	98.21	98.94	100.40	99.88	98.94	99.10	99.10	98.24	98.24	100.40	98.72	99.77
Ba	1285	1305	354	820	1770	643	982	1505	496	400	1170	1035	567
Rb	75.5	66.4	58.5	57.0	83.0	58.9	56.2	70.2	48.7	36.7	51.0	64.6	55.7
Th	13.5	9.0	11.4			10.6	14.0	13.0	13.7	1.0		11.5	9.9
Nb	4.5	4.3	5.5	21.0	19.0	6.4	5.7	5.7	6.4	2.0	5.0	5.1	2.9
Sr	430	356	316	446	568	311	319	264	300	183	381	231	198
Zr	236	205	269	491	262	254	227	233	274	79	296	163	27
Y	8.3	6.1	31.5	9.0	15.0	16.8	16.4	7.3	22.3	35.2	44.0	11.4	10.4
Cr	10		10			20		10					
V	42	32	46			53	51	33	37	9		23	14
Ni			8			11	7			5		9	
Co	7	5	7			5	5	5	5	5		3	3
Pb	41	23	22			24	35	49	20	19		27	24
Cu	9		6			9		6	5				
Zn	173	72	86			82	68	209	62	24		55	36
Cs	1.50	1.38	2.17			1.64	1.01	1.71	1.02	0.46		0.56	0.59
Ga	21.2	19.4	17.7			18.6	17.8	18.6	17.6	16.5		17.2	15.6
Sn	4	2	1			1	1	6	1	1		1	1
Ta	0.4	0.4	0.3			0.5	0.4	0.4	0.4	0.2		0.2	0.2
Hf	6.2	5.6	7.3			6.8	5.9	6.0	7.6	3.1		4.7	0.9
U	2.99	2.61	3.31			2.25	2.93	2.34	3.76	3.19		1.97	0.99
La	55.4	36.5	45.2			42.4	52.2	54.6	46.8	10.6		28.4	13.6
Ce	102.0	66.3	87.5			78.7	98.3	103.0	93.0	14.4		58.2	27.8
Pr	10.2	6.8	9.6			8.6	10.2	10.8	10.2	3.1		5.9	3.0
Nd	34.5	23.0	35.6			31.5	36.1	37.1	37.4	13.2		21.2	11.8
Sm	5.06	3.25	6.45			5.61	5.86	5.65	7.05	2.96		3.83	2.47
Eu	1.02	0.94	2.25			1.73	1.71	1.00	1.72	1.53		0.97	0.97
Gd	3.85	2.74	6.06			4.98	5.13	4.28	6.35	3.61		3.42	2.16
Tb	0.42	0.30	0.88			0.65	0.62	0.41	0.89	0.62		0.45	0.29
Dy	1.60	1.26	5.02			3.09	2.90	1.62	4.36	4.14		2.11	1.74
Ho	0.32	0.22	1.16			0.63	0.57	0.25	0.80	0.99		0.38	0.37
Er	0.82	0.63	3.57			1.80	1.49	0.72	2.09	3.06		1.00	1.14
Tm	0.11	0.09	0.52			0.26	0.18	0.09	0.32	0.54		0.12	0.18
Yb	0.71	0.60	3.19			1.61	1.16	0.66	1.76	3.19		0.75	1.30
Lu	0.18	0.16	0.53			0.28	0.18	0.16	0.30	0.55		0.16	0.23

Prl: protolith (undeformed granitoid); Sd: slightly deformed granitoid; Prm: protomylonite; Myl: mylonite.

The Sr isotopic ratios were normalized to $^{86}Sr/^{88}Sr = 0.1194$; replicate analyses of $^{87}Sr/^{86}Sr$ for the NBS987 standard give a mean value of 0.71028 ± 0.00006 (2σ), with measured Sr blanks of 5 ng. Nd isotopic ratios were normalized to $^{146}Nd/^{144}Nd = 0.72190$. The averages of $^{143}Nd/^{144}Nd$ for La Jolla and BCR-1 standards were 0.511847 ± 0.00005 (2σ) and 0.512662 ± 0.00005 (2σ), respectively. The blanks measured < 0.03 ng Nd. Isotopic analyses of Sr and Nd were carried out on a multicollector VG 354 Micromass and Finnigan-MAT 262 mass spectrometers, respectively. Initial Sr and Nd isotopic ratios were calculated to an age of 1105 Ma, as deduced from U–Pb SHRIMP data. Analytical results are given in Table 5.

Undeformed/slightly deformed granitoid (sample TM1-05) has a $(^{87}Sr/^{86}Sr)_{1105}$ ratio of 0.70543 and $(^{143}Nd/^{144}Nd)_{1105}$ ratio of 0.511424, with a εNd value of +4.2. This initial Sr signature is slightly more radiogenic than those calculated for other Grenvillian granitoids present in the Cuyania terrane (Juchi orthogneiss, 1108 Ma, 0.70217–0.70337, Varela et al., 2003; Pie de Palo orthogneisss, 1021 ± 12 Ma, 0.7045, Pankhurst and Rapela, 1998; Las Matras granitoid, ≈1200 Ma, 0.7030, Sato et al., 2000) and even the nearby 774 ± 6 Ma A-type granitoid (0.70309, Baldo et al., 2006). Nevertheless, in terms of εNd values, the ETG presents a rather primitive signature, only comparable with that of the A-type granitoid (+4.2 to +5.0) and more primitive than the other Grenvillian granitoids present in the region (+2.3 to +2.8 for the Juchi orthogneiss and +1.6 to +1.8 for the Las Matras granitoid).

Data from moderately deformed ETG (sample TM3-05) suggests mainly open system behavior for the Sr isotopes during deformation, with $(^{87}Sr/^{86}Sr)_{1105} = 0.69840$, $(^{143}Nd/^{144}Nd)_{1105} = 0.511332$ and εNd +2.4. Moreover, highly deformed ETG mylonite (sample TM7-05) has a more radiogenic signature $(^{87}Sr/^{86}Sr)_{1105} = 0.71655$, $(^{143}Nd/^{144}Nd)_{1105} = 0.511160$ and εNd −1.0 which could be the consequence of high fluid-rock interaction between the granitoid and the host rocks during mylonitization processes. In fact, highly deformed granitoid (sample TM7-05) has a higher $^{147}Sm/^{144}Nd$

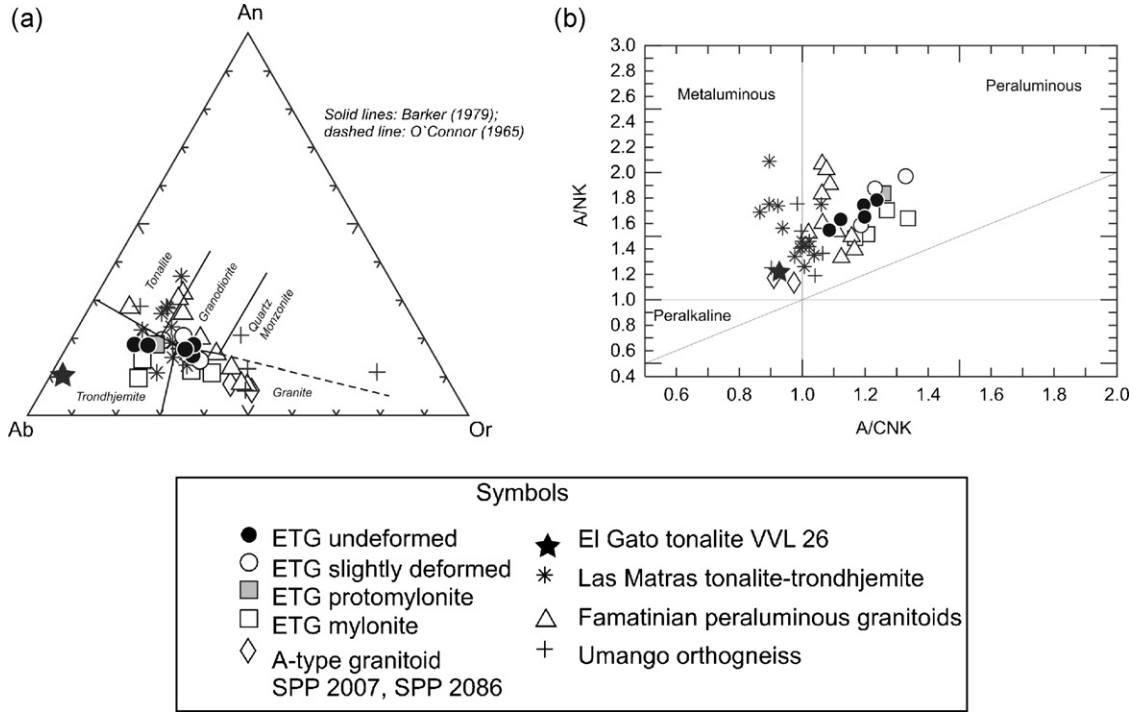

Fig. 7. (a) Geochemical classification diagram of granitoids after O'Connor (1965) modified by Barker (1979), based on the normative Ab, An, and Or proportions. (b) Plot of A/CNK $(Al_2O_3/CaO + Na_2O + K_2O)_{molar}$ *vs.* A/NK $(Al_2O_3/Na_2O + K_2O)_{molar}$ for the ETG and other Grenvillian granitoids (El Gato Tonalite, Vujovich et al., 2004; Las Matras granitoids, Sato et al., 2000 and Sierra de Umango orthogneiss, Varela et al., 2003). A-type granitoid (Baldo et al., 2006) and Famatinian peraluminous granitoids from the Western Sierras Pampeanas (Dahlquist et al., 2007) are also represented.

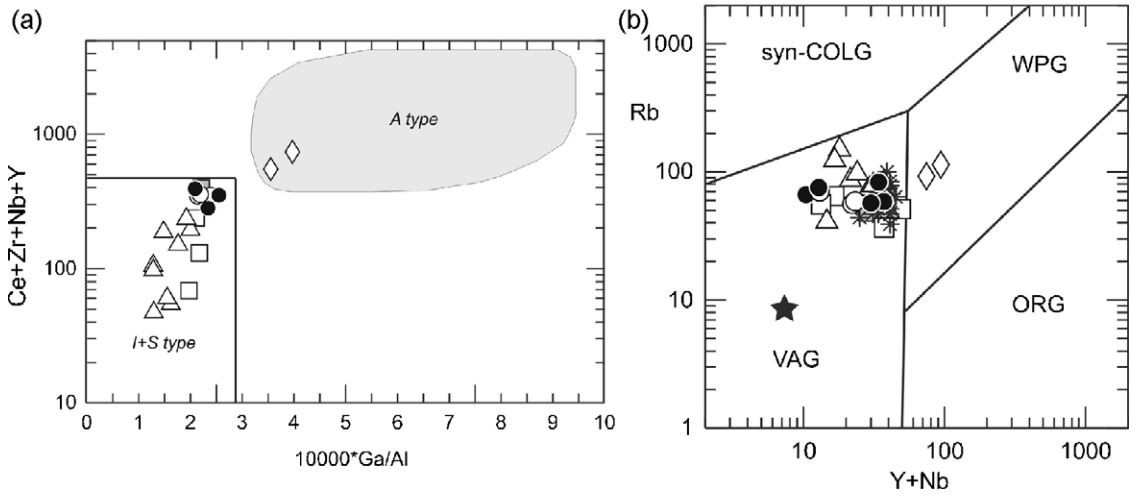

Fig. 8. Discrimination diagrams for granitoids. (a) Plot of $10^4 \times$ Ga/Al *vs.* (Ce + Zr + Nb + Y) showing the I + S type and A-type granitoids fields. (b) (Y + Nb) *vs.* Rb diagram (Pearce et al., 1984) showing the fields of syn-collisional granites (syn-COLG), within plate granites (WPG), volcanic arc granites (VAG) and ocean-ridge granites (ORG). Symbols as in Fig. 7.

ratio and a lower Zr/Y ratio (≈2.2) compared with undeformed samples. For the purpose of petrogenetic considerations, only the isotopic signature of sample TM1-05 (tabular-shaped, 5 m wide, undeformed to slightly deformed tonalite) was considered. The single-stage model ages (T_{DM} and $T_{DM\text{-}2}$) calculated for the undeformed rock is 1.20 or 1.34 Ga according to the different calculations applied (Table 5). Nevertheless, for granitoid rocks with $^{147}Sm/^{144}Nd$ ratios more than 10% different from that of the average continental crust, as in the ETG case, a two-stage Nd model age (T_{2DM} in Table 5) seems to be more appropriate to estimate the average crustal residence age of the protolith (see Li et al., 2003). The T_{2DM} model ages for the ETG is 1.39 Ga (Table 5), slightly older than model ages calculated using single-stage models.

7. Discussion

7.1. Age and geotectonic relationships for the ETG

The crystallization sequence deduced from microscopic textural criteria indicates that quartz, oligoclase, biotite and muscovite (Ms_1) are the earliest (magmatic) phases. Microperthitic K-feldspar is later in the sequence and textural relationships suggest that it replaced plagioclase. Metamorphic retrograde/alteration effects are locally widespread and include: partial to total replacement of plagioclase by very fine-grained sericite ± epidote, biotite replaced by secondary muscovite (Ms_2) accompanied by iron-titanium oxide segregation, albitization of plagioclase, substitution of K-feldspar

Table 5
Analytical results of Rb–Sr and Sm–Nd-isotopes from the El Tigre Granitoid (ETG), Sierra de Pie de Palo, Western Sierras Pampeanas, Argentina.

	Rb (ppm)	Sr (ppm)	$^{87}Rb/^{86}Sr$	$^{87}Sr/^{86}Sr$	$(^{87}Sr/^{86}Sr)_o$	εSri	Sm (ppm)	Nd (ppm)	$^{147}Sm/^{144}Nd$	$^{143}Nd/^{144}Nd$	$(^{143}Nd/^{144}Nd)_o$	εNd_{CHURt}	T_{DM} (Ga)	T_{CHUR} (Ga)	T_{DM-2} (Ga)	T_{2DM} (Ga)
TM1-05	64.50	419.02	0.44569	0.712474	0.705425	113.19	5.52	34.20	0.097547	0.5121311	0.5114236	4.15	1.20	0.78	1.34	1.39
TM3-05	50.64	353.84	0.41410	0.704953	0.698404	6.43	7.35	42.71	0.104128	0.5120874	0.5113322	2.36	1.33	0.91	1.48	1.53
TM7-05	33.15	183.72	0.52304	0.724820	0.716548	288.43	5.72	27.06	0.127765	0.5120870	0.5111604	−1.00	1.66	1.22	1.88	1.80

εNd_{CHURt} calculated using present-day values for a chondritic uniform reservoir (CHUR) of $^{147}Sm/^{144}Nd = 0.1967$ and $^{143}Nd/^{144}Nd = 0.512638$. Jacobsen and Wasserburg (1984).
T_{DM} calculated using the depleting mantle data model values of $(^{147}Sm/^{144}Nd) = 0.222$ and $(^{143}Nd/^{144}Nd) = 0.513114$. Michard et al. (1985).
T_{CHUR} calculated using the present-day CHUR model values of Jacobsen and Wasserburg (1984).
T_{DM-2} using the depleting mantle data model values of $(^{147}Sm/^{144}Nd) = 0.2137$ and $(^{143}Nd/^{144}Nd) = 0.513151$. Goldstein and Jacobsen (1988).
T_{2DM} using the Keto and Jacobsen (1987) formulation, with $f_{Sm/Nd}$ values for continental crust and depleted mantle of −0.4 and 0.08592, respectively.

Fig. 9. Chondrite-normalized (Nakamura, 1974) REE patterns for (a) representative samples of the undeformed ETG (black circle), slightly deformed granitoid (white circle) and highly deformed ETG mylonite (white square). (b) REE pattern of representative ETG undeformed-slightly deformed rocks compared with other Grenvillian rocks from the Cuyania terrane, Argentina. Symbols as in Fig. 7.

by microcline, and chloritization of biotite. Metamorphic garnet is partially replaced by chlorite ± epidote + Fe-oxides. Occasionally, fine-grained biotite rims garnet and replaces it along cracks suggesting that the formation of garnet was followed by a retrograde episode of biotite growth during low-pressure–low-temperature metamorphism. A local overprinted mylonitic event is inferred from zones with intensive grain-size reduction, the presence of porphyroclast relicts immersed in a well-foliated, very fine-grained matrix, and stretching lineation development. Microstructural analysis suggests the predominance of brittle and low-temperature plastic processes during mylonitic deformation.

Consequently, textural and mineralogical evidence indicates that the ETG experienced amphibolite to greenschist facies metamorphism after igneous crystallization, followed by later strong deformation restricted to narrow mylonite zones and partial dynamic recrystallization under lower-T conditions.

The SHRIMP U–Pb zircon age obtained in this study allows us to constrain the crystallization age of the ETG to 1105.5 ± 4.1 Ma. Igneous and metaigneous rocks with ages between 1020 and 1110 Ma belonging to the Grenvillian Basement of the Western Sierras Pampeanas (Fig. 1) are dioritic to granodioritic intrusions (*ca.* 1079 Ma, U–Pb zircon, McDonough et al., 1993), orthogneisses (1091–938 Ma, U–Pb zircon, McDonough et al., 1993; 1021 ± 12 Ma, Rb–Sr isochron, Pankhurst and Rapela, 1998) and migmatites (1027 ± 59 Ma, Rb–Sr isochron, Varela and Dalla Salda, 1993) in the Sierra de Pie de Palo, the orthogneisses from Juchi, Sierra de

Umango (1108 ± 13 Ma, U–Pb zircon, Varela et al., 2003) and the anorthosites of Sierra de Maz and Sierra del Espinal (1070 ± 41 Ma, U–Pb SHRIMP zircon, Casquet et al., 2004). The tectonic model proposed by Vujovich and Kay (1998) for the SPP, invokes a Mesoproterozoic oceanic suprasubduction zone setting for the Pie de Palo Complex that collided with a continental block during the Grenville Orogeny. Collision was followed by the formation of a Mesoproterozoic, dominantly felsic arc, whose magmas erupted through the thickened crust. Minor felsic arc rocks, mainly tonalite and granodiorite sills and dykes included in the Pie de Palo Complex, are thought to represent the younger felsic arc stage (Vujovich et al., 2004). According to the obtained U–Pb SHRIMP age (1105 Ma), the slightly peraluminous ETG could have been emplaced during a Mesoproterozoic tectono-thermal event and would be part of the magmatic complex forming the Grenvillian basement of the Western Sierras Pampeanas.

$^{40}Ar/^{39}Ar$ ages obtained both in biotite as well as in muscovite, reflect subsolidus re-equilibration processes after crystallization. A biotite plateau age of 910 ± 20 Ma could be explained as a post-magmatic (metamorphic?) thermal event in which biotite and garnet could be recrystallized, probably during a not yet well constrained Grenvillian metamorphic event. In this sense, it is worth remarking that Sato et al. (2000) suggest a Neoproterozoic thermal event to justify previously obtained K-Ar ages in biotite from tonalites of 869 ± 17 Ma. Nevertheless, the obtained biotite ages could also be explained as the consequence of single processes of cooling due to slow exhumation rates after plutonic emplacement. This thermal event could have developed previous to the Neoproterozoic crustal rifting episode that eventually led to the break-up of Rodinia (Baldo et al., 2005, 2006).

The 641 ± 3 Ma age calculated by dating muscovite may not have any geological significance due the disturbed $^{40}Ar/^{39}Ar$ pattern that could be explained by (i) impurities in the muscovite crystals giving mixed and erroneous ages or (ii) mixing between Ms_1 and Ms_2 as previously showed.

ETG mylonites developed as a result of strong ductile deformation mainly restricted to narrow shear zones oriented NE-E, whose dextral shear sense (Castro de Machuca et al., 2008) is compatible with the NNE striking regional Las Pirquitas Thrust. The K/Ar age of 473 ± 10 Ma on very fine-grained recrystallized white-mica suggests that shearing, developed under greenschist facies conditions, occurred close to the Lower-Middle Ordovician in the SPP. This event was probably related to ductile thrusting dated to slightly before 460 Ma (Casquet et al., 2001). Additionally, Ramos and Vujovich (2000) suggest that the Las Pirquitas Thrust developed before 395.7 ± 0.2 Ma. Moreover, recent $^{40}Ar/^{39}Ar$ ages of *ca.* 515 Ma obtained on amphiboles from mylonite–ultramylonite in the Las Pirquitas Thrust (Mulcahy et al., 2007) could indicate the earliest phase of deformation responsible for juxtaposition of the Pie de Palo complex and the El Quemado Formation of the Caucete Group. Younger ages of *ca.* 464 Ma from an amphibolite somewhere within the complex shear zone (Ramos et al., 1998) together with our new K/Ar ages of 473 ± 10 Ma, would then reflect the age of penetrative D_2 deformation (Van Staal et al., 2005) and accretion of the Cuyania terrane during the Famatinian Orogeny.

7.2. Constraints on possible magma source

The geochemistry of the ETG allows us to establish some constraints on the genesis of magmas from which it crystallized. Major elements classified these rocks mostly as trondhjemites and granites, with $Na_2O/K_2O = 1–2$, $Al_2O_3 \approx 16\%$, Sr = 311–568 ppm, an absence of a positive Sr anomaly in primordial mantle-normalized trace element diagrams (not shown in the present paper), relatively low Sr/Y ratios and $Yb_N > 10$ in undeformed rocks (e.g. sample TM1-05). All these geochemical features are mostly characteristic of the

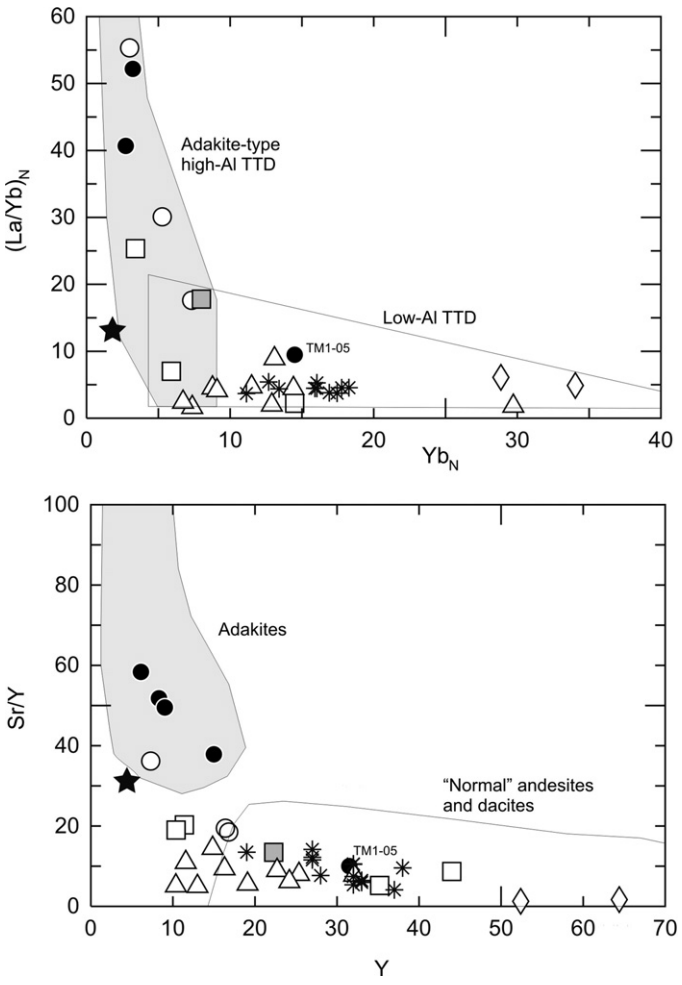

Fig. 10. (a) $(La/Yb)_N$ *vs.* Yb_N and (b) Sr/Y *vs.* Y diagrams discriminating between adakites and high-Al TTD with respect to normal andesites and low-Al TTD compositions (from Drummond and Defant, 1990 and Martin, 1999). Symbols as in Fig. 7.

so-called low-Al TTD (trondhjemite–tonalite–dacite, Fig. 9), interpreted by Drummond and Defant (1990) as the result of partial melting from a plagioclase-bearing basaltic source without garnet as a residual phase. Nevertheless, lower Y and Yb values have been observed in deformed to highly deformed granitoids. The lower contents of these elements could be related to the lower garnet amount observed, which may be due to the different deformational behaviors with respect to the more plastic mica-rich matrix. These low Y and Yb ETG rocks would consequently plot mostly in the adakite field (Fig. 10), but must be interpreted as having been generated from low-pressure melting of a mafic source with garnet-free residues. Moreover, geochemical signatures of the ETG are similar to those found by Sato et al. (2000) for the Las Matras Block (interpreted by these authors as low-Al TTD), except in the metaluminous character of the latter granitoids compared with the slightly peraluminous signature of the ETG (Figs. 7–9) with primary muscovite (Ms_1) and metamorphic garnet and muscovite (Ms_2) as peraluminous phases. However, the presence of these two minerals could be explained in relation to a metamorphic rather than igneous origin, both minerals (garnet and muscovite Ms_2) having recrystallized under amphibolite facies metamorphic conditions after igneous emplacement. A similar explanation to justify the presence of accessory muscovite and garnet in 1 Ga peraluminous granitoids has been proposed by Pandit et al. (2003). According to these authors, muscovite could be formed from subsolidus metamorphic

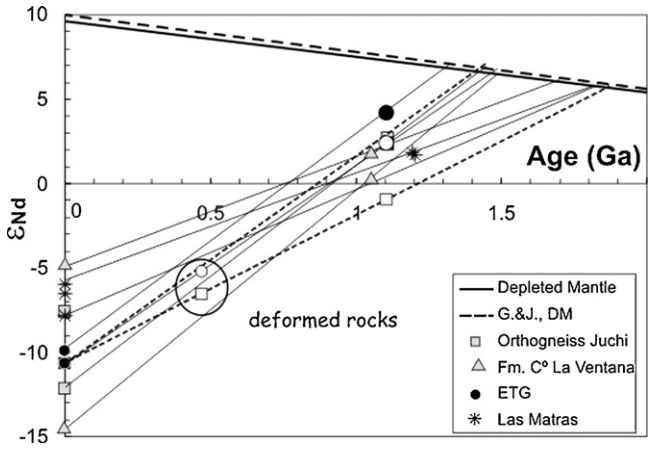

Fig. 11. *T vs.* εNd diagram for the 1105 Ma ETG and other granitoids of the Cuyania terrane, Argentina, related to the Grenvillian magmatic event. Symbols as in Fig. 7.

recrystallization of sericitic feldspar alteration produced during late-magmatic hydrothermal processes. Moreover, El Gato tonalitic sill, exposed at Quebrada El Gato and Quebrada Las Pirquitas close to our study area (Fig. 1b), and plotting in the trondhjemite field in Fig. 7a, shows a distinctive trace element pattern with lower REE contents (Fig. 9b), suggesting differences in the source and petrogenetic processes involved, with the presence of garnet as a residual phase. In fact, the low high-field strength element ratios observed in this rock has been interpreted as a consequence of an oceanic rather than a continental setting (Vujovich et al., 2004 and references therein).

The ETG isotopic initial ratios with $(^{87}Sr/^{86}Sr)_{1105}$ values of 0.70543 and εNd of +4.2 are similar to the Sr initial isotopic ratios found in the Sierra de Pie de Palo orthogneiss (0.7045 ± 0.0003, Pankhurst and Rapela, 1998) but contrast with the meta-aluminous Juchi orthogneiss (1108 Ma, $(^{87}Sr/^{86}Sr)_o$ <0.7040 and εNd = +2.3 to +2.7, Varela et al., 2003) and the meta-aluminous low-Al Las Matras TTG (≈1200 Ma, $(^{87}Sr/^{86}Sr)_o$ 0.7030, εNd = +1.6 to +1.8, Sato et al., 2000). The ETG isotopic signatures indicate a rather depleted and juvenile (immature) source for its origin, in concordance with the immature source proposed by Pankhurst and Rapela (1998) for the parent magma of the Sierra de Pie de Palo orthogneiss.

Nd model ages using both single-stage and two-stage modeling (T_{DM}, $T_{DM\text{-}2}$, T_{2DM}) calculated for undeformed ETG samples (1.2–1.39 Ga, Fig. 11 and Table 5) are similar to those obtained by Rapela et al. (2005) from para-amphibolites of the Difunta Correa Sequence, and relatively younger than those obtained by Varela et al. (2003) in the orthogneiss Juchi (1.45–1.48 Ga). They are only slightly older than the 1105 Ma SHRIMP U–Pb crystallization zircon age obtained here. This short time span between the Nd model ages and the crystallization age could be interpreted in an adakite genesis model similar to that proposed by Martin (1999) for the Archean TTG. According to this model, during the Mesoproterozoic young oceanic crust could have been subducted under a very high geothermal gradient, generating subducted slab melts at shallow pressure conditions, giving a garnet-free but plagioclase-bearing residue. Nevertheless, partial melting of juvenile underplating basaltic rocks at lower pressure under a high thermal regime with a high degree of hornblende fractionation could also generate peraluminous magmas (see Wareham et al., 1997 and references therein) similar to those the ETG could derived from. In any case, this thermal anomaly necessary to melt a mafic protolith could be associated with the hypothetical 1.1 Ga global episode of higher mantle heat flow proposed by Kumar et al. (2007). Crystallization of these low-pressure basaltic source melts could be the source of the low-Al trondhjemite–tonalite–granodiorite of both the ETG and the Las Matras Block. Consequently, the ETG is a Grenville-age felsic peraluminous igneous body cropping out in the Sierra de Pie de Palo and represents part of the crystalline basement of the Western Sierras Pampeanas.

8. Conclusions

The El Tigre Granitoid (ETG), located in the southwestern Sierra de Pie de Palo (31°31′30″S–68°15′12″W), crops out as small, tabular to lenticular vein-like intrusions into the metasedimentary rocks of the Pie de Palo Complex. The ETG is geochemically characterized by its moderate peraluminousity (ASI = 1.09–1.33; A/CNK >1.1), plotting mostly in the granite–trondhjemite fields on an Ab–An–Or diagram. Relationships between trace elements suggest the classical setting of granitoids produced in a convergent plate setting under a compressive tectonic regime.

Textural and mineralogical evidence indicates that the ETG experienced amphibolite to greenschist facies metamorphism after igneous crystallization, followed by later strong deformation restricted to narrow mylonite zones (ETG shear zone) and partial dynamic recrystallization under lower-T conditions. The NE-E striking ETG shear zone has a dextral shear sense compatible with the kinematics of the related NNE striking regional Las Pirquitas Thrust. The K/Ar age of 473 ± 10 Ma on very fine-grained recrystallized white-mica indicates that shearing occurred close to the Lower-Middle Ordovician.

A U–Pb SHRIMP crystallization age on zoned igneous zircon of 1105.5 ± 4.1 Ma suggests that the ETG could be part of the magmatic complex forming the Grenvillian basement of the Western Sierras Pampeanas. Moreover, the $(^{87}Sr/^{86}Sr)_{1105}$ values of 0.70543 and εNd of +4.2 indicate a rather immature source for its origin. Geochemical and isotopic signatures of the ETG could be explained by low-pressure partial melting processes from a basaltic source under high geothermal gradient conditions. This thermal anomaly could be associated with the 1.1 Ga global period of enhanced mantle plume activity, developing widespread global magmatism (Kumar et al., 2007). Consequently, the ETG is a Grenville-age felsic peraluminous igneous body cropping out in the Sierra de Pie de Palo, which represents part of the crystalline basement of the Cuyania terrane of the Western Sierras Pampeanas.

Acknowledgments

Comments, corrections and suggestions by Drs. Pablo D. González, Wulf Mueller and an anonymous referee led to significant improvements on the earlier manuscript. The authors also wish to thank to Lic Lorena Previley for help in the field work and Dr. Jacobus Le Roux for the English revision of the manuscript. This research was supported by CONICET (Argentina), Grant PIP 5649.

References

Arancibia, G., Matthews, S., Pérez de Arce, C., 2006. K–Ar and $^{40}Ar/^{39}Ar$ geochronology of supergene processes in Atacama Desert, northern Chile: tectonic and climatic relations. J. Geol. Soc. London 163 (1), 107–118.

Astini, R., Benedetto, J.L., Vaccari, N.E., 1995. The Early Paleozoic evolution of the Argentine Precordillera as a Laurentian rifted, drifted, and collided terrane: a geodynamic model. Geol. Soc. Am. Bull. 107, 253–273.

Baldo, E., Casquet, C., Galindo, C., 1998. Datos preliminares sobre el metamorfismo de la Sierra de Pie de Palo, Sierras Pampeanas Occidentales (Argentina). Geogaceta 24, 39–42.

Baldo, E., Dahlquist, J., Rapela, C., Casquet, C., Pankhurst, R., Galindo, C., Fanning, C., 2005. Early Ordovician peraluminous magmatim in the Sierra de Pie de Palo (Western Sierras Pampeanas): geotectonic implications. In: Pankhurst, R., Veiga, G. (Eds.), Gondwana 12: Geological and Biological Heritage of Gondwana, Abstracts. Academia Nacional de Ciencias, Córdoba, Argentina, p. 57.

Baldo, E., Casquet, C., Pankhurst, R., Galindo, C., Rapela, C., Fanning, C., Dahlquist, J., Murra, J., 2006. Neoproterozoic A-type magmatism in the Western Sierras Pampeanas (Argentina): evidence for Rodinia break-up along a proto-Iapetus rift? Terra Nova 18 (6), 388–394.

Barker, F., 1979. Trondhjemite: definition, environment and hypothesis of origin. In: Barker, F. (Ed.), Trondhjemites, Dacites and Related Rocks. Elsevier, Amsterdam, pp. 1–12.

Casquet, C., Baldo, E., Pankhurst, R.J., Rapela, C.W., Galindo, C., Fanning, C.M., Saavedra, J., 2001. Involvement of the Argentine Precordillera Terrane in the Famatinian Mobile Belt: geochronological (U–Pb SHRIMP) and metamorphic evidence from Sierra de Pie de Palo. Geology 29, 703–706.

Casquet, C., Pankhurst, R.J., Rapela, C.W., Galindo, C., Dahlquist, J., Baldo, E., Saavedra, J., González Casado, J.M., Fanning, C.M., 2004. Grenvillian massif-type anorthosites in the Sierras Pampeanas. J. Geol. Soc. London 162, 9–12.

Castro de Machuca, B., Arancibia, G., Previley, L., Pontoriero, S., Morata, D., 2008. Ordovician mylonites from Mesoproterozoic granitoid, Sierra de Pie de Palo, Western Sierras Pampeanas, San Juan Province. In: Proceedings of the 6th South American Symposium on Isotope Geology, San Carlos de Bariloche, Argentina, CD-Rom edition.

Dahlquist, J.A., Galindo, C., Pankhurst, R.J., Rapela, C.W., Alasino, P.H., Saavedra, J., Fanning, C.M., 2007. Magmatic evolution of the Peñón Rosado granite: petrogenesis of garnet-bearing granitoids. Lithos 95, 177–207.

Drummond, M.S., Defant, M.J., 1990. A model for trondhjemite–tonalite–dacite genesis and crustal growth via slab melting: archean to modern comparisons. J. Geophys. Res. 95 (B13), 21503–21521.

Finney, S.C., 2007. The parautochthonous Gondwanan origin of the Cuyania (greater Precordillera) terrane of Argentina: a re-evaluation of evidence used to support an allochthonous Laurentian origin. Geol. Acta 5, 127–158.

Galindo, C., Casquet, C., Baldo, E., Pankhurst, R., Rapela, C., Saavedra, J., 2004. Sr, C and O isotope geochemistry of carbonates from Sierra de Pie de Palo and other Western Sierras Pampeanas (Argentina). Stratigraphy and constraints on the derivation of the Precordillera Terrane. Precambrian Res. 131, 57–71.

Goldstein, S.J., Jacobsen, S.B., 1988. Nd and Sr isotopic systematics of river water suspended material: implications for crustal evolution. Earth Planet. Sci. Lett. 87, 249–265.

Jacobsen, S.B., Wasserburg, G.J., 1984. Sm–Nd isotopic evolution of chondrites and achondrites. Earth Planet. Sci. Lett. 67, 137–150.

Kay, S., Orell, S., Abruzzi, J.M., 1996. Zircon and whole-rock Nd–Pb isotopic evidence for a Grenville age and a Laurentian origin for the basament of the Precordillera in Argentina. J. Geol. 104, 637–648.

Keller, M., 1999. Argentine Precordillera: Sedimentary and Plate Tectonic History of a Laurentian Crustal Fragment in South America. Geological Society of America, Special Paper, 341, 131 pp.

Keto, L.S., Jacobsen, S.B., 1987. Nd and Sr isotopic variations of Early Paleozoic oceans. Earth Planet. Sci. Lett. 84, 27–41.

Kumar, A., Heaman, L.H., Manikyamba, C., 2007. Mesoproterozoic kimberlites in south India: a possible link to ~1.1 Ga global magmatism. Precambrain Res. 154, 192–204.

Li, X.H., Li, Z.X., Ge, W., Zhou, H., Li, W., Liu, Y., Wingate, M.T.D., 2003. Neoproterozoic granitoids in South China: crustal melting above a mantle plume at ca. 825 Ma? Precambrian Res. 122, 45–83.

Martin, H., 1999. Adakitic magmas: modern analogues of Archean granitoids. Lithos 46, 411–429.

McDonough, M.R., Ramos, V.A., Isachsen, C.E., Bowring, S.A., Vujovich, G.I., 1993. Edades preliminares de circones del basamento de la sierra de Pie de Palo, Sierras Pampeanas Occidentales de San Juan: sus implicancias para los modelos del supercontinente proterozoico de Rodinia. In: Proceedings of the 12th Congreso Geológico Argentino and 2nd Congreso de Exploración de Hidrocarburos Mendoza, Argentina, Actas 3, 340–342.

Michard, A., Gurriet, P., Soudant, M., Albarede, F., 1985. Nd isotopes in French Phanerozoic shales: external vs. internal aspects of crustal evolution. Geochim. Cosmochim. Acta 49, 601–610.

Mulcahy, S., Roeske, S., McClelland, W., Nomade, S., Renne, P., 2007. Cambrian initiation of the Las Pirquitas thrust of the western Sierras Pampeanas, Argentina: implications for the tectonic evolution of the proto-Andean margin of South America. Geology 35 (5), 443–446.

Naipauer, M., Cingolani, C.A., McClelland, W.C., Vujovich, G., Ellis, J.R., 2005. U–Pb (LA-ICP-MS) ages on detrital zircon grains from Angacos limestone siliciclastic levels (Caucete Group), San Juan province, Argentina: provenance implications for the Cuyania terrane. In: Proceedings of the 5th South American Symposium on Isotope Geology, Abstracts: 225–228, Punta del Este, Uruguay, CD-Rom edition.

Naipauer, M., Vujovich, G., Cingolani, C.A., McClelland, W.C., 2009. Detrital zircon analysis from the Neoproterozoic-Cambrain sedimentary cover (Cuyania terrane), Sierra Pie de Palo, Argentina: evidence of a rift and passive margin system? J. South Am. Earth Sci., doi:10.1016/j.jsames.2009.10.001.

Nakamura, N., 1974. Determination of REE, Ba, Mg, Na and K in carbonaceous and ordinary chondrites. Geochim. Cosmichim. Acta 38, 757–775.

O'Connor, J.T., 1965. A classification for quartz-rich igneous rocks based on feldspar ratios. U.S. Geological Survey, Professional Paper, 525B, pp. 79–84.

Pandit, M.K., Carter, L.M., Ashwal, L.D., Tucker, R.D., Torsvik, T.H., Jamtveit, B., Bhushan, S.K., 2003. Age, petrogenesis and significance of 1 Ga granitoids and related rocks from the Sendra area, Aravalli Craton, NW India. J. Asian Earth Sci. 22, 363–381.

Pankhurst, R.J., Rapela, C.W., 1998. The proto-Andean margin of Gondwana: an introduction. In: Pankhurst, R.J., Rapela, C.W. (Eds.), The Proto-Andean Margin of Gondwana. Geological Society of London, Special Publication, 142, pp. 1–9.

Passchier, C.W., Trouw, R.A.J., 2005. Microtectonics, Second ed. Springer, Berlin, 366 pp.

Pearce, J.A., Harris, N.B.W., Tindle, A.G., 1984. Trace element discrimination diagrams for the tectonic interpretation of granitic rocks. J. Petrol. 25, 956–983.

Ramos, V.A., 1999. Las Provincias Geológicas del Territorio Argentino. In: Caminos, R. (Ed.), Geología Argentina. IGRM-SEGEMAR, Buenos Aires, Anales 29 (3), pp. 41–96.

Ramos, V.A., 2004. Cuyania, an exotic block to Gondwana: review of a historical success and the present problems. Gondwana Res. 7, 1009–1026.

Ramos, V., Vujovich, G., 2000. Hoja Geológica 3169-IV San Juan, provincia de San Juan. Boletín No. 243. Servicio Geológico Minero Argentino, Buenos Aires, 82 p.

Ramos, V., Dallmeyer, R., Vujovich, G., 1998. Time constraints on the early Paleozoic docking of the Precordillera, central Argentina. In: Pankhurst, R.J., Rapela, C.W. (Eds.), The Proto-Andean Margin of Gondwana. Geological Society of London, Special Publication 142, pp. 143–158.

Rapela, C., Pankhurst, R.J., Casquet, C., Fanning, C.M., Galindo, C., Baldo, E., 2005. Datación U–Pb SHRIMP de circones detríticos en paranfibolitas neoproterozoicas de la secuencia Difunta Correa (Sierras Pampeanas Occidentales, Argentina). Geogaceta 38, 227–230.

Sato, A.M., Ticky, H., Llambías, E.J., Sato, K., 2000. The Las Matras tonalitic–trondhjemitic pluton, central Argentina: Grenvillian-age constraints, geochemical characteristics, and regional implications. J. South Am. Earth Sci. 13, 587–610.

Sato, A.M., Tickyj, H., Llambias, E.J., Basei, M.A.S., González, P.D., 2004. Las Matras Block, Central Argentina (37°S–67°W): the Southernmost Cuyania terrane and its relationship with the Famatinian Orogeny. Gondwana Res. 7, 1077–1087.

Sato, K., Tassinari, C.G.C., Kawashita, K., Petronillo, L., 1995. O método geocronológico Sm–Nd no IG-USP e suas aplicações. An. Acad. Bras. Cienc. 67, 313–336.

Steiger, R.N., Jager, E., 1977. Subcommission on geochronology: convention on the use of decay constants in geo- and cosmochronology. Earth Planet. Sci. Lett. 36, 359–362.

Streckeisen, A., 1976. To each plutonic rock its proper name. Earth Sci. Rev. 12, 1–33.

Tassinari, C.C.G., Medina, J.G.C., Pinto, M.C.S., 1996. Rb–Sr and Sm–Nd geochronology and isotope geochemistry of Central Iberian Metassedimentary Rocks (Portugal). Geologie en Mijnbouw 75, 69–79.

Thomas, W.A., Astini, R.A., 1996. The Argentine Precordillera: a traveler from Ouachita embayment of North America Laurentia. Science 273, 752–757.

Van Staal, C., Vujovich, G., Davis, W., 2005. Evolution of structures in a continental subduction channel: an example from the Sierra de Pie de Palo, Cuyania terrane, Argentina. In: Pankhurst, R., Veiga, G. (Eds.), Gondwana 12: Geological and Biological Heritage of Gondwana, Abstracts. Academia Nacional de Ciencias, Córdoba, Argentina, p. 362.

Varela, R., Dalla Salda, L., 1993. Geocronología Rb–Sr de metamorfitas y granitoides del extremo sur de la Sierra de Pie de Palo, San Juan. Revista de la Asociación Geológica Argentina 47, 271–276.

Varela, R., Sato, A.M., Basei, M., Siga, O., 2003. Proterozoico medio y Paleozoico inferior de la Sierra de Umango, antepaís andino (29°S), Argentina: edades U–Pb y caracterizaciones isotópicas. Rev. Geol. Chile 30, 265–284.

Varela, R., Basei, M.A.S., Sato, A.M., Siga Jr., W., González, P.D., Campos Neto, M. da Costa, Cingolani, C.A., 2008. New U–Pb data for Sierra de Umango, Andean foreland at 29°S, and geodynamic implications. In: Proceedings of the 6th South American Symposium on Isotope Geology, San Carlos de Bariloche, Argentina, CD-Rom edition.

Vaughan, A.P.M., Pankhurst, R.J., 2008. Tectonic overview of the West Gondwana margin. Gondwana Res. 13, 150–162.

Vujovich, G.I., Kay, S.M., 1998. A Laurentian Grenville-age oceanic arc/back-arc terrane in the Sierra de Pie de Palo, Western Sierras Pampeanas, Argentina. In: Pankhurst, R.J., Rapela, C.W. (Eds.), The Proto-Andean Margin of Gondwana. Geological Society of London, Special Publication 142, pp. 159–179.

Vujovich, G., van Staal, C.R., Davis, W., 2004. Age Constraints on the Tectonic Evolution and Provenance of the Pie de Palo Complex, Cuyania Composite Terrane, and the Famatinian Orogeny in the Sierra de Pie de Palo, San Juan, Argentina. Gondwana Res. 7, 1041–1056.

Wareham, C.D., Millar, I.L., Vaughan, A.P.M., 1997. The generation of sodic granite magmas, western Palmer Land, Antarctic Peninsula. Contrib. Mineral. Petrol. 128, 81–96.